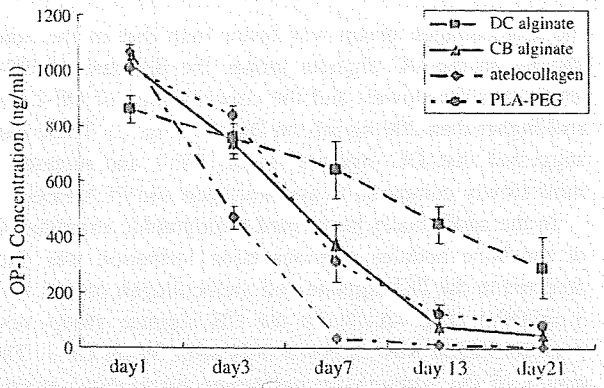

Fig. 3 OP-1 release from each carrier material/OP-1 (30 μg) composite was measured over time by a commercial BMP-7 ELISA kit. With each carrier material, the maximum concentration of OP-1 was detected on Day 1 and it decreased afterward. The decline was slowest in the DC alginate group.

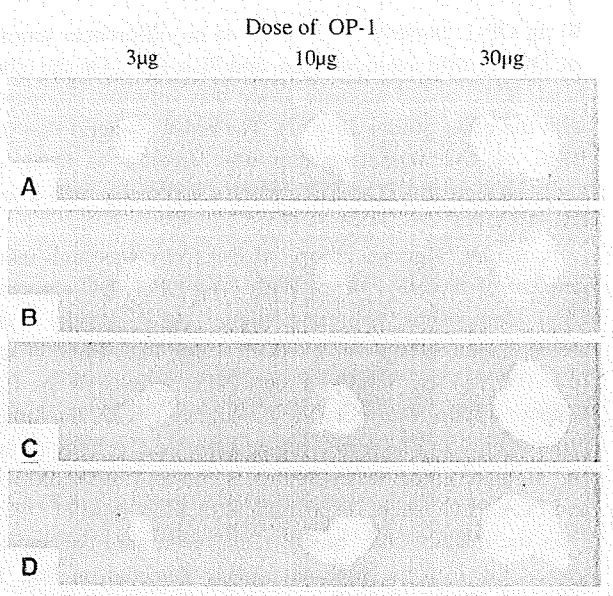

Fig. 4A–D The carriers for OP-1 tested were (**A**) DC alginate, (**B**) CB alginate, (**C**) atelocollagen, and (**D**) PLA-PEG. Soft xray photographs of ectopic bone induced by OP-1 (3, 10, or 30 μg) show bone formation with the DC alginate/OP-1 composite is equivalent or superior to that induced by the other carrier/OP-1 composites.

surrounding cancellous bone that contained hematopoietic bone marrow, and no inflammatory change was observed (Fig. 5A–D). These additional results were compatible with the results of BMC and ALP activity, suggesting that DC alginate can be an equivalent or superior carrier for a low dose of OP-1 compared with atelocollagen and PLA-PEG.

Discussion

Various materials have already been evaluated as carriers for BMPs, but they all have some disadvantages as mentioned previously. This study was designed to examine whether alginate, a material with no animal product content, is an equivalent or superior carrier for OP-1(BMP-7) compared with atelocollagen and PLA-PEG. Specifically we hypothesized: (1) BMC of bone nodules ectopically induced by DC alginate/OP-1 composite and/or CB alginate/OP-1 composite are equivalent or superior to those by atelocollagen and PLA-PEG; (2) ALP activity of bone nodules ectopically induced by DC alginate/OP-1 composite and/or CB alginate/OP-1 composite are equivalent or superior to those by atelocollagen and PLA-PEG; and (3) DC alginate and/or CB alginate have appropriate in vitro release kinetics of OP-1 equivalent to atelocollagen and PLA-PEG.

This study has several limitations. First, DC alginate was originally approved for clinical use as a cutaneous wound dressing [8, 37]. Therefore, its biodegradability and immunogenicity are unclear during use at a deeper site. Second, in the histological examination, DC alginate remained at the center of the new ectopic bone, indicating it had not degraded within 3 weeks. Although no inflammatory reaction was found, longer observation will be necessary before this material can be used with confidence at deeper sites. Third, ALP activity is a marker for osteoblastic differentiation, and is high in the early stage of osteoblast lineage. ALP activity is not necessarily parallel to the activity of bone formation. Fourth, in the release study, a commercial BMP-7 ELISA kit can only detect the amount of BMP-7(OP-1) protein, but cannot evaluate the activity of OP-1. The result of a release test may not reflect the actual activity of OP-1 released from carriers in vivo.

To determine whether DC alginate and/or CB alginate are equivalent or superior carriers for OP-1 compared with atelocollagen and PLA-PEG, we measured BMC of ectopic bone nodules as a primary research question. A previous study [24] reported that BMC of the ectopic bone induced by PLA-PEG/BMP-2 composite is about 6 mg higher than that by atelocollagen/BMP-2 composite. In our study, the BMC of DC alginate/OP-1 (3 μg) composite was about 6 mg higher than that of the atelocollagen/OP-1 (3 μg) composite and even much higher than that of CB alginate and PLA-PEG. The result of BMC measurement suggested that DC alginate is a highly effective carrier that enhances the bone-inducing effect of OP-1 even when OP-1 content is low.

The result of ALP activity measurement was compatible with the result of BMC, which reinforced the hypothesis that DC alginate is an equivalent or superior carrier compared with the other materials. Upon histological examination, not only trabecular bone but also normal hematopoietic bone marrow was observed, and we found

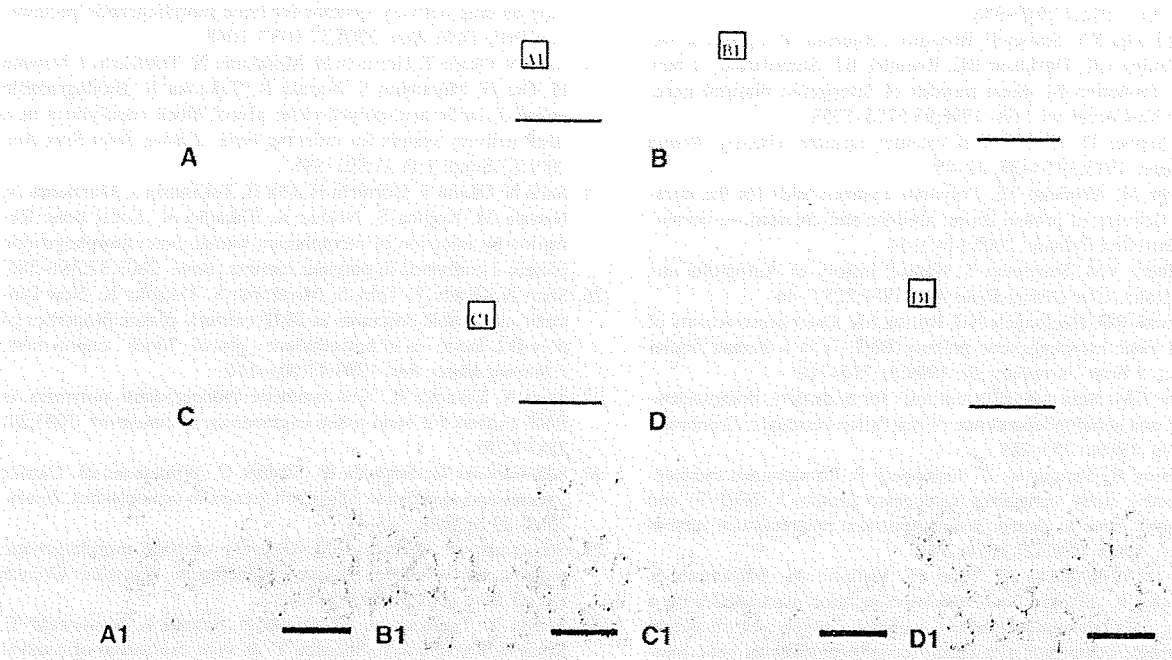

Fig. 5A–D Representative photomicrographs of the ectopic bone formation induced by OP-1 (30 μg) are shown (**A**, A1: DC alginate; **B**, B1: CB alginate; **C**, C1: atelocollagen; **D**, D1: PLA-PEG) (**A–D**: stain, hematoxylin and eosin; original magnification, ×10; scale bar = 2 mm; A1–D1: stain, hematoxylin and eosin; original magnification, ×100; scale bar = 200 μm). Irrespective of the carrier material, the newly formed bone had a thin cortex surrounding cancellous bone that contained highly cellular bone marrow.

no accumulation of inflammatory cells, such as monocyte/macrophages. The histological appearance of the ectopic bone induced by DC alginate/OP-1 composite seemed similar to that by atelocollagen/OP-1 composite, which is considered a safe biomaterial in terms of immunological response. These data suggested that DC alginate appears likely a safe material with no inflammatory response even when used in a deep site.

In contrast, CB alginate achieved relatively poor bone formation, especially with a low dose of OP-1. DC alginate and CB alginate only differ in the mode of crosslinking, but the release of OP-1 from these two alginates was quite different. It is known crosslinking by divalent cations forms a characteristic egg box structure that is suitable for trapping proteins in alginate [9]. Thus, the difference of bone formation between these two types of alginate may be partly due to a difference in their ability to retain OP-1 and release it slowly. It is also known the number of carboxyl residues in DC alginate is larger than that in CB alginate. The carboxyl residues induce apatite nucleation followed by the deposition of hydroxyapatite crystals on the alginate [35]. Furthermore, the Ca^{2+} contained in DC alginate can be utilized for new calcified bone, which is an advantage compared with CB alginate.

In conclusion, our data suggest DC alginate, a material with no animal product content that is approved by the FDA and other authorities, is a safe and potent carrier for OP-1. It is of note that DC alginate strongly potentiates osteoinduction of OP-1 even at a low dose. Thus, its use may reduce the cost of OP-1-based bone regeneration therapy.

Acknowledgments We thank Stryker Biotech, Smith & Nephew, Koyo Sangyo Co, Ltd, Johnson & Johnson, and Taki Chemicals Co, Ltd, for kindly providing the chemicals and materials.

References

1. Bach FH, Fishman JA, Daniels N, Proimos J, Anderson B, Carpenter CB, Forrow L, Robson SC, Fineberg HV. Uncertainty in xenotransplantation: individual benefit versus collective risk. *Nature Med.* 1998;4:141–144.
2. Bonadio J, Smiley E, Patil P, Goldstein S. Localized, direct plasmid gene delivery in vivo: prolonged therapy results in reproducible tissue regeneration. *Nature Med.* 1999;5:753–759.
3. Burkus JK, Dorchak JD, Sanders DL. Radiographic assessment of interbody fusion using recombinant human bone morphogenetic protein type 2. *Spine.* 2003;28:372–377.
4. Butler D, Wadman M, Lehrman S, Schiermeier Q. Last chance to stop and think on risks of xenotransplants. *Nature.* 1998;391:320–324.

5. Delustro F, Dasch J, Keefe J, Ellingsworth L. Immune responses to allogeneic and xenogeneic implants of collagen and collagen derivatives. *Clin Orthop Relat Res.* 1990;260: 263–279.
6. Einhorn TA. Enhancement of Fracture-Healing. *J Bone Joint Surg Am.* 1995;77:940–956.
7. Fang J, Zhu YY, Smiley E, Bonadio J, Rouleau JP, Goldstein SA, McCauley LK, Davidson BL, Roessler BJ. Stimulation of new bone formation by direct transfer of osteogenic plasmid gene. *Proc Natl Acad Sci USA.* 1996;93:5753–5758.
8. Gensheimer D. A review of calcium alginate. *Ostomy Wound Manage.* 1993;39:34–38, 42–43.
9. George M, Abraham TE. Polyionic hydrocolloids for the intestinal delivery of protein drugs: alginate and chitosan—a review. *J Controlled Release.* 2006;114:1–14.
10. Goldberg VM, Stevenson S. Natural history of Autografts and Allografts. *Clin Orthop Relat Res.* 1987;225:7–16.
11. Greesink RG, Hoefnagels NH, Bulstra SK. Osteogenic activity of OP-1 bone morphogenetic protein (BMP-7) in a human fibular defect. *J Bone Joint Surg Br.* 1999;81:710–718.
12. Jarque CM, Bera AK. Efficient tests for normality, homoscedasticity and serial independence of regression residuals. *Economics Letters.* 1980;6:255–259.
13. Johnsson R, Stromqvist B, Aspenberg P. Randomized radiostereometric study comparing osteogenic protein-1 (BMP-7) and autograft bone in human noninstrumented posterolateral lumbar fusion. *Spine.* 2002;27:2654–2661.
14. Kato M, Namikawa T, Terai H, Hoshino M, Miyamoto S, Takaoka K. Ectopic bone formation in mice associated with a lactic acid/dioxanone/ethylene glycol copolymer-tricalcium phosphate composite with added recombinant human bone morphogenetic protein-2. *Biomaterials.* 2006;27:3927–3933.
15. Kato M, Toyoda H, Namikawa T, Hoshino M, Terai H, Miyamoto S, Takaoka K. Optimized use of biodegradable polymer as a carrier material for the local delivery of recombinant human bone morphogenetic protein-2 (rhBMP-2). *Biomaterials.* 2006;27:2035–2041.
16. Kirker-Head CA. Potential applications and delivery strategies for bone morphogenetic proteins. *Adv Drug Deliv Rev.* 2000;43: 65–92.
17. Lee DD, Tofighi A, Aiolova M, Chakravarthy P, Catalano A, Majahad A, Knaack D. Alpha-BSM: a biomimetic bone substitute and drug delivery vehicle. *Clin Orthop Relat Res.* 1999;367: S396–S405.
18. Matsumine A, Myoui A, Kusuzaki K, Araki N, Seto M, Yoshikawa H, Uchida A. Calcium hydroxyapatite ceramic implants in bone tumor surgery: a long-term follow-up study. *J Bone Joint Surg Br.* 2004;86:719–725.
19. Miyamoto S, Takaoka K, Okada T, Yoshikawa H, Hashimoto J, Suzuki S, Ono K. Evaluation of polylactic acid homopolymers as carriers for bone morphogenetic protein. *Clin Orthop Relat Res.* 1992;278:274–285.
20. Miyamoto S, Takaoka K, Okada T, Yoshikawa H, Hashimoto J, Suzuki S, Ono K. Polylactic acid-polyethylene glycol block copolymer: a new biodegradable synthetic carrier for bone morphogenetic protein. *Clin Orthop Relat Res.* 1993;294:333–343.
21. Nemzek JA, Arnoczky SP, Swenson CL. Retroviral transmission by the transplantation of connective-tissue allografts. *J Bone Joint Surg Am.* 1994;76:1036–1041.
22. Ohgushi H, Dohi Y, Toshikawa T, Tamai S, Tabata S, Suwa Y. In vitro bone formation by rat marrow cell culture. *J Biomed Mater Res.* 1996;32:341–348.
23. Saito N, Murakami N, Takahashi J, Horiuchi H, Ota H, Kato H, Okada T, Nozaki K, Takaoka K. Synthetic biodegradable polymers as drug delivery systems for bone morphogenetic proteins. *Adv Drug Deliv Rev.* 2005;57:1037–1048.
24. Saito N, Okada T, Horiuchi H, Murakami N, Takahashi J, Nawata M, Ota H, Miyamoto S, Nozaki K, Takaoka K. Biodegradable poly-D,L-lactic acid-polyethylene glycol block copolymers as a BMP delivery system for inducing bone. *J Bone Joint Surg Am.* 2001;83 Suppl 1(Pt 2):S92–S98.
25. Saito N, Okada T, Horiuchi H, Ota H, Takahashi J, Murakami N, Nawata M, Kojima S, Nozaki K, Takaoka K. Local bone formation by injection of recombinant human bone morphogenetic protein-2 contained in polymer carriers. *Bone.* 2003;32:381–386.
26. Saito N, Okada T, Toba S, Miyamoto S, Takaoka K. New synthetic absorbable polymers as BMP carriers: plastic properties of poly-D,L-lactic acid-polyethylene glycol block copolymers. *J Biomed Mater Res.* 1999;47:104–110.
27. Saito N, Takaoka K. New synthetic biodegradable polymers as BMP carriers for bone tissue engineering. *Biomaterial.* 2003;24: 2287–2293.
28. Schmidmaier G, Schwabe P, Strobel C, Wiidemann B. Carrier systems and application of growth factors in orthopaedics. *Injury.* 2008; 39 Suppl 2:S37–43.
29. Seeherman H, Wozney J M. Delivery of bone morphogenetic proteins for orthopedic tissue regeneration. *Cytokine Growth Factor Rev.* 2005;16:329–345.
30. Suzuki Y, Tanihara M, Nishimura Y, Suzuki K, Yamawaki Y, Kudo H, Kakimaru Y, Shimizu Y. In vivo evaluation of a novel alginate dressing. *J Biomed Mater Res.* 1999;48:522–527.
31. Takaoka K, Koezuka M, Nakamura H. Telopeptide-depleted bovine skin collagen as a carrier for bone morphogenetic protein. *J Orthop Res.* 1991;9:902–907.
32. Takaoka K, Nakahara H, Yoshikawa H, Masuhara K, Tsuda T, Ono K. Ectopic bone induction on and in porous hydroxyapatite combined with collagen and bone morphogenetic protein. *Clin Orthop Relat Res.* 1988;234:250–254.
33. Tamai N, Myoui A, Tomita T, Nakase T, Tanaka J, Ochi T, Yoshikawa H. Novel hydroxyapatite ceramics with an interconnective porous structure exhibit superior osteoconduction in vivo. *J Biomed Mater Res.* 2002;59:110–117.
34. Tamura S, Kataoka H, Matsui Y, Shionoya Y, Ohno K, Michi KI, Takahashi K, Yamaguchi A. The effects of transplantation of osteoblastic cells with bone morphogenetic protein (BMP)/carrier complex on bone repair. *Bone.* 2001;29:169–175.
35. Tanahashi M, Matsuda T. Surface functional group dependence on apatite formation on self-assembled monolayers in a simulated body fluid. *J Biomed Mater Res.* 1997;34:305–315.
36. Urist MR. Bone formation by autoinduction. *Science.* 1965;150: 893–899.
37. Vanstraelen P. Comparison of calcium sodium alginate (KALTOSTAT) and porcine xenograft (E-Z DERM) in the healing of split-thickness skin graft donor sites. *Burns.* 1992;18:145–148.
38. Wang EA, Rosen V, D'Alessandro JS, Baudny M, Cordes P, Harada T, Israel DI, Hewick RM, Kerns KM, LaPan P, Luxenberg DP, McQuaid D, Moutsatsos IK, Nove J, Wozeny EA. Recombinant human bone morphogenetic protein induces bone formation. *Proc Natl Acad Sci USA.* 1990;87:2220–2224.

Journal of Clinical Pharmacy and Therapeutics (2009) 34, 355–361 doi:10.1111/j.1365-2710.2009.01046.x

PHARMACOGENETICS

Genetic polymorphisms in folate pathway enzymes as a possible marker for predicting the outcome of methotrexate therapy in Japanese patients with rheumatoid arthritis

H. Hayashi* MSc, C. Fujimaki* BS, T. Daimon† PhD, S. Tsuboi‡ MD, T. Matsuyama§ BS and K. Itoh* PhD

**Department of Clinical Pharmacology & Genetics, †Department of Drug Evaluation & Informatics, School of Pharmaceutical Sciences, University of Shizuoka, ‡Department of Rheumatology and §Department of Pharmacy, Shizuoka Kousei Hospital, Shizuoka, Japan*

SUMMARY

Background: Low-dose methotrexate (MTX) therapy is widely used in the treatment of rheumatoid arthritis (RA). Though the difference in response to MTX between patients with RA is large, the factors that contribute to this variability remain unclear.

Objective: We aimed to identify those factors with a particular emphasis on the pharmacogenetics of MTX.

Method: We evaluated the association of possible factors, including genetic polymorphisms of folate metabolic pathway enzymes, with the cumulative value of C-reactive protein, an index of MTX anti-inflammatory efficacy, in 87 Japanese patients with RA.

Results: Polymorphisms of the reduced folate carrier gene (*RFC*) G80A and of the γ-glutamylhydrolase gene (*GGH*) C−401T were more closely associated ($\beta = 2{\cdot}1194$, $P = 0{\cdot}0017$) than other polymorphisms, with the anti-inflammatory response to MTX.

Conclusion: Patients with RA having *RFC* 80A and *GGH* −401T alleles were less responsive to MTX than those with *RFC* 80A and without *GGH* −401T alleles. Thus, this data may be useful for guiding treatment of RA patients with MTX.

Received 13 April 2008, Accepted 25 July 2008
Correspondence: K. Itoh, PhD, Professor, Department of Clinical Pharmacology & Genetics, School of Pharmaceutical Sciences, University of Shizuoka, 52-1 Yada, Suruga-ku, Shizuoka 422-8526, Japan. Tel.: +81 54 264 5673; fax: +81 54 264 5673; e-mail: itohk@u-shizuoka-ken.ac.jp

Keywords: C-reactive protein, γ-glutamylhydrolase, methotrexate, polymorphism, reduced folate carrier, rheumatoid arthritis

INTRODUCTION

Methotrexate (MTX) is an antifolate that is widely used to treat hyper-immune disorders [e.g., rheumatoid arthritis (RA), and cancers, including childhood acute lymphoblastic leukemia] (1–6). In general, low-dose MTX, usually administered orally as a weekly pulse, is first-line therapy for RA that is unresponsive to non-steroidal anti-inflammatory drugs (7); however, it is associated with over-immunosuppression, which may lead to bone marrow depression and increased susceptibility to infection (8). Though the response to low-dose MTX shows wide inter-patient variability (9–11), the contributing factors remain unclear. However, the differences in dosage requirement are usually attributed to inter-patient differences in pharmacokinetics and pharmacodynamics parameters.

Intestinal absorption of MTX and its uptake into target cells are mainly controlled by the polymorphic reduced folate carrier gene (*RFC*). A previous report demonstrated that in patients with leukemia treated with MTX, a single nucleotide polymorphism (SNP) G80A was associated with higher MTX concentration (12). However, a recent study reported that *RFC* G80A SNP affects MTX treatment outcome in RA (13) and that remission of RA symptoms was significantly higher in *RFC* 80AA carriers in comparison with 80GG individuals (odds ratio = 3·32).

After cell entry, MTX is rapidly converted to γ-glutamyl polyglutamates (PGs) by folylpolyglutamate synthetase, which sequentially adds up to six glutamyl residues to MTX (14–16). MTX-PGs are potent inhibitors of dihydrofolate reductase (DHFR) resulting in depletion of reduced folates, the cofactors for thymidylate synthase (17). γ-Glutamyl hydrolase (GGH) is a lysosomal peptidase that catalyses the removal of γ-linked polyglutamates, converting long-chain MTX-PGs into short-chain MTX-PGs and ultimately to MTX, allowing folate to be exported from the cell (18, 19). Several SNPs have been identified in the *GGH* gene (e.g., C−401T, G−354T, and C452T) (20). Cheng *et al.* reported that *GGH* C452T (Thr127Ile) significantly reduced the activity of GGH in hydrolyzing long-chain MTX-PGs, and led to MTX-PGs accumulation in acute lymphoblastic leukemia blasts of patients treated with high-dose MTX (21). Allele frequency in this SNP vary significantly between different ethnic groups and we reported the genotype distribution and allele frequency of *GGH* C452T in a Japanese population (22). All of the promoter polymorphisms analyzed enhanced GGH expression (20). *GGH* C−401T has been shown to be associated with altered accumulation of MTX-PGs in RA patients treated with MTX (23).

Methylenetetrahydrofolate reductase (MTHFR) has a critical role in the folate cycle. It converts 5,10-methylene-tetrahydrofolate (methyl-donor in thymidine monophosphate synthesis) to 5-methyltetrahydrofolate (carbon donor required for methionine synthesis). Moreover, two common SNPs in the *MTHFR* gene (C677T and A1298C) have been found to influence the efficacy and toxicity of MTX (24, 25).

Current MTX dosing algorithms do not include the genetic background of patients with RA, although it could affect the response to MTX. Thus, the aim of this study was to examine what factors, including SNPs of these genes, were associated with the anti-inflammatory response to low-dose MTX therapy in Japanese patients with RA.

MATERIALS AND METHODS

Patients

We recruited 219 patients with RA in our study from the Department of Rheumatology, Shizuoka Kousei Hospital. RA was diagnosed according to American College of Rheumatology criteria. Eighty-seven patients who had been receiving weekly pulse of MTX for ≥12 months, and were undergoing analysis of blood biochemistry at least every 2 months during the previous 12 months, were selected. Patients receiving concurrent therapy known to affect MTX dosing (e.g., infliximab, etanercept, tacrolimus, cyclosporine) were excluded. Written informed consent was obtained from all patients after a detailed briefing of the purpose and protocol of the study. Age, sex, body weight, additional medical problems, and concurrent medications were recorded. A blood sample was taken for serum C-reactive protein (CRP) and creatinine measurement and *RFC*, *GGH* and *MTHFR* genotyping. We used the CRP level as a marker of inflammatory status in RA because CRP is highly sensitive in this respect, and is not affected by sex, age, or other proteins. The area under the curve of the serial CRP measurements (CRP-AUC) was calculated to quantify total inflammatory status during 12 months of MTX treatment. CRP-AUC is associated with the outcome of RA treatment (26, 27). Creatinine clearance was calculated according to the Cockcroft–Gault formula (28). Glucocorticoids doses were calculated as prednisolone-equivalent doses, where 5 mg prednisolone was equivalent to 20 mg hydrocortisone, 750 μg dexamethasone, or 750 μg betamethasone (29). This study was approved by the Ethics Committee of Shizuoka Kousei Hospital and the University of Shizuoka.

Genotyping assays

Leukocyte genomic DNA was extracted directly from whole blood using a QIAamp DNA Blood Mini Kit (Qiagen, Hilden, Germany). Genotyping was performed using polymerase chain reaction–restriction fragment length polymorphism (PCR–RFLP) and allele-specific PCR (AS-PCR) assays. Primer sequences, PCR conditions and restriction enzymes are shown in Table 1. PCR products and restriction enzyme digestion products were electrophoresed on 2–4% agarose gels with ethidium bromide and viewed under UV light.

Data analyses

To identify factors associated with CRP-AUC, the data were analyzed with respect to age, sex, body

Table 1. Details of genotyping methods for six SNPs in *RFC*, *GGH* and *MTHFR*

Genes	SNPs	Methods[a]	Primers[b]	Annealing temperatures	Digestion enzymes	Digestion temperatures	Ref.
RFC	G80A	PCR–RFLP	F: 5′- AGT GTC ACC TTC GTC CCC TC -3′ R: 5′- CTC CCG CGT GAA GTT CTT -3′	60 °C	*Hha* I	37 °C	23,26
GGH	C−401T	PCR–RFLP	F: 5′- TAG AAT CCC CTG CCA GCC TCC TCG -3′ R: 5′- TAA GCG GAG ACT CTG GAA ACG ACT -3′	63 °C	*Bsl* I	55 °C	20 (Modified)
	G−354T	PCR–RFLP	F: 5′- TAG AAT CCC CTG CCA GCC TCC TCG -3′ R: 5′- TAA GCG GAG ACT CTG GAA ACG ACT -3′	63 °C	*Afl* II	37 °C	20 (Modified)
	C452T	PCR–RFLP	F: 5′- GTG CCT ATT TGG TTA TGA CA -3′ R: 5′- CTA CTT ACT AAT CCT GCC CA -3′	55 °C	*Ase* I	37 °C	20,22
MTHFR	C677T	PCR–RFLP	F: 5′- TGA ACA GGT GGA GGC CAG CCT CT -3′ R: 5′- AGG ACG GTG CGG TGA GAG TG -3′	65 °C	*Hinf* I	37 °C	38
	A1298C	AS-PCR	F: 5′- GGA GGA GCT GAC CAG TGA ATA-3′ (for A allele) F: 5′- GGA GGA GCT GAC CAG TGA ATC -3′ (for C allele) R: 5′- CCA CTC CAG CAT CAC TCA CT -3′	55 °C			38 (Modified)

[a]PCR–RFLP and AS-PCR are the abbreviations of polymerase chain reaction–restriction fragment length polymorphism and allele-specific PCR assay, respectively.
[b]F and R are the abbreviations of forward primer and reverse primer, respectively.

weight, creatinine clearance, MTX dose, glucocorticoids dose, and six SNPs of genes coding for three enzymes involved in the folate pathways. CRP-AUC was logarithmically transformed because it had a left-skewed distribution. Factors significantly associated with CRP-AUC in a univariate analysis were included in a multivariate model and a multiple linear regression was used to adjust for the effects of the factors. To evaluate the effects of the combination of the SNPs, the main effect and first-order interaction effect terms of the SNPs were included in the regression models. In statistics, the 'main effect' term is used in the model when one factor is independent of the effect of the other factors, whereas the 'interaction effect' is used when the effects of two or more factors are not simply additive. Such a term implies that the effect of one factor depends on the values of one or more other factors. $P < 0{\cdot}05$ was considered statistically significant. Reported values of P were two-sided. The statistical analyses were performed using R version 2.6.1 (http://www.r-project.org/).

RESULTS

Patient characteristics and genotypes

Eighty-seven Japanese patients with RA met the eligibility criteria (Table 2). The frequencies of the polymorphisms were in Hardy–Weinberg equilibrium.

Effect of each factor on CRP-AUC

In the univariate analysis (Table 3) sex, age and glucocorticoid dose were found to be significantly associated with the CRP-AUC. The results of univariate analysis on the effects of the combination of SNPs are shown in Table 4. The main effect of *RFC* 80GA and AA (vs. GG) was found to be significant; the interaction effects between *RFC* 80AA and *GGH* −401CT/TT (vs. CC) and between RFC 80AA and MTHFR 677CT had values of $P < 0{\cdot}1$. All other main and interaction effects had a value of $P > 0{\cdot}1$. The results of multivariate analysis are shown in Table 5. Age ($P = 0{\cdot}0495$), MTX dose ($P = 0{\cdot}0205$), the effects of *RFC* 80AA ($P = 0{\cdot}0243$) and *GGH* −401 CT/TT ($P = 0{\cdot}0129$), and interaction effect between *RFC* 80AA and *GGH* −401 CT/TT ($P = 0{\cdot}0017$) were significant. The interaction effects between *RFC*

Table 2. Characteristics and genetic polymorphisms of 87 Japanese patients with RA

Age (years)	66 (35–89)
Sex Male/Female (*n*, %)	13/74 (15/85)
Body weight (kg)	47·0 (29·6–80·0)
Creatinine clearance (mL/min)	64·8 (23·9–119·5)
Methotrexate dose (mg/week)	6·0 (2·0–13·3)
Glucocorticoids dose (equivalent to prednisolone, mg/day)	3·8 (0–10·0)
CRP-AUC (mg·1 year/dL)	256 (37–2638)
RFC G80A	
Genotype GG/GA/AA (*n*, %)	21/35/31 (24/40/36)
Allele G/A (*n*, %)	77/97 (44/56)
GGH C–401T	
Genotype CC/CT/TT (*n*, %)	52/32/3 (60/37/3)
Allele C/T (*n*, %)	136/38 (78/22)
GGH G–354T	
Genotype GG/GT/TT (*n*, %)	73/13/1 (84/15/1)
Allele G/T (*n*, %)	159/15 (91/9)
GGH C452T	
Genotype CC/CT/TT (*n*, %)	78/9/0 (90/10/0)
Allele C/T (*n*, %)	165/9 (95/5)
MTHFR C677T	
Genotype CC/CT/TT (*n*, %)	32/40/15 (37/46/17)
Allele C/T (*n*, %)	104/70 (60/40)
MTHFR A1298C	
Genotype AA/AC/CC (*n*, %)	47/32/8 (54/37/9)
Allele A/C (*n*, %)	126/48 (72/28)

Values are median (range) except for sex, genotypes and alleles.

Table 3. Results of univariate analysis of patient characteristics

Factors	Estimate of regression parameters	*P*
Sex (Male vs. Female)	0·7949	0·0283
Age	0·2647	0·0132
Body weight	0·0670	0·5370
Creatinine clearance	−0·0918	0·3980
Methotrexate dose	0·1855	0·0855
Glucocorticoids dose	0·2509	0·0191

80AA and *GGH* −401 CT/TT are shown in the interaction plot (Fig. 1). It can be seen that the effect of *RFC* 80 genotype for *GGH* 401CC is different to those for *GGH* −401CT/TT (Fig. 1). This suggests that patients with RA having *RFC* 80A and *GGH*

Table 4. Results of univariate analysis on effects of combination of SNPs

Main and interaction effects of SNPs	Estimate of regression parameter	*P*
RFC 80GA	−2·3820	0·0449
RFC 80AA	−2·7844	0·0188
GGH −401CT/TT	−1·4124	0·1792
GGH −354GT/TT	0·1066	0·9524
GGH 452CT	−0·0984	0·9624
MTHFR 677CT	−0·9377	0·3787
MTHFR 677TT	−0·2619	0·8386
MTHFR 1298AC/CC	0·0578	0·9532
RFC 80GA : *GGH* −401CT/TT	0·9712	0·2748
RFC 80AA : *GGH* −401CT/TT	2·2920	0·0239
RFC 80GA : *GGH* −354GT/TT	0·4324	0·7740
RFC 80AA : *GGH* −354GT/TT	0·4975	0·6739
RFC 80GA : *GGH* 452CT	0·1500	0·9239
RFC 80AA : *GGH* 452CT	−0·4757	0·7901
RFC 80GA : *MTHFR* 677CT	1·4738	0·1331
RFC 80AA : *MTHFR* 677CT	1·7264	0·0877
RFC 80GA : *MTHFR* 677TT	0·8753	0·5173
RFC 80AA : *MTHFR* 677TT	−1·3090	0·6004
RFC 80GA : *MTHFR* 1298AC/CC	0·6312	0·5139
RFC 80AA : *MTHFR* 1298AC/CC	0·7240	0·4290
GGH −401CT/TT : *GGH* −354GT/TT	0·3925	0·8322
GGH −401CT/TT : *MTHFR* 677CT	0·2093	0·7864
GGH −401CT/TT : *MTHFR* 677TT	−0·0668	0·9539
GGH −401CT/TT : *MTHFR* 1298AC/CC	−0·4508	0·5602
GGH −354GT/TT : *GGH* 452CT	0·3448	0·8963
GGH −354GT/TT : *MTHFR* 677CT	0·0263	0·9840
GGH −354GT/TT : *MTHFR* 677TT	1·2248	0·5950
GGH −354GT/TT : *MTHFR* 1298AC/CC	−0·3748	0·7484

The colon (:) denotes an interaction effect term. There was no other combination of SNPs.

−401T alleles were less responsive to MTX than those with *RFC* 80A and without *GGH* −401T alleles.

DISCUSSION

Methotrexate is one of the most widely used anti-cancer and anti-inflammatory agents. Low-dose MTX administered orally as a weekly pulse, has been used extensively in RA therapy (1, 6). It has been reported that SNPs in genes of folate metabolic pathway enzymes affect the efficacy and

Table 5. Results of multivariate analysis

Factors	Estimate of regression parameter	*P*
Sex (Male vs. Female)	0·3990	0·2858
Age	0·0216	0·0495*
Methotrexate dose	0·1431	0·0205*
Glucocorticoids dose	0·0603	0·3083
RFC 80GA	−1·2527	0·0906
RFC 80AA	−1·7036	0·0243*
GGH −401CT/TT	−1·6594	0·0129*
MTHFR 677CT	−0·4829	0·5036
MTHFR 677TT	0·1437	0·8656
RFC 80GA : *GGH* −401CT/TT	0·8156	0·2066
RFC 80AA : *GGH* −401CT/TT	2·1194	0·0017*
RFC 80GA : *MTHFR* 677CT	0·2300	0·7834
RFC 80AA : *MTHFR* 677CT	0·7300	0·3772
RFC 80GA : *MTHFR* 677TT	0·0561	0·9522
RFC 80AA : *MTHFR* 677TT	0·5917	0·6083
GGH −401CT/TT : *MTHFR* 677CT	0·6842	0·2473
GGH −401CT/TT : *MTHFR* 677TT	0·3992	0·5889

The colon (:) denotes an interaction effect term.
*Significance of ($P < 0·05$).

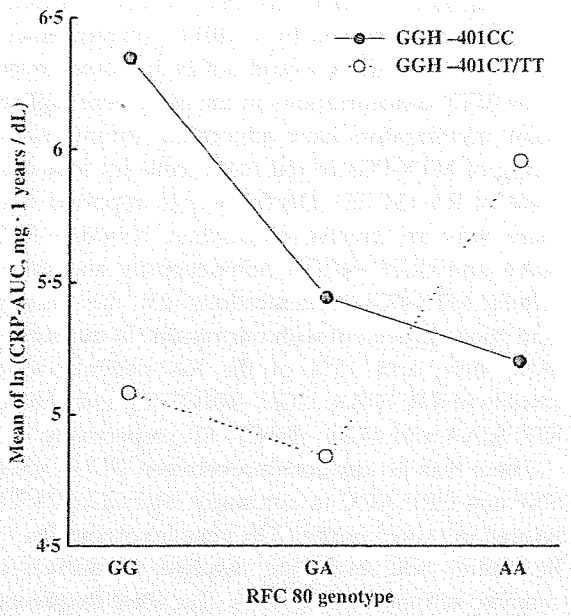

Fig. 1. Interaction plot showing the effects of GGH C-401T genotype and RFC G80A genotype on the mean of the natural logarithm of CRP-AUC in patients with RA receiving low-dose, weekly pulse of MTX. The closed symbol denotes GGH-401CT/TT genotype, whereas the open symbol denotes GGH-401CC genotype.

toxicity of MTX (12, 21, 23–25); however, there are only few reports on the relationship between the interaction effect of these SNPs and MTX efficacy in Japanese patients with RA. Thus, in the present study we evaluated the effects of factors, including the SNPs of folate metabolic pathway enzymes genes such as *RFC*, *GGH* and *MTHFR*, on CRP-AUC, as one of the indices of the anti-inflammatory efficacy of MTX. Our study, suggested that age, MTX dose, the main effects of *RFC* 80AA and *GGH* −401CT/TT genotypes, and the interaction effect between *RFC*80AA and *GGH* −401CT/TT genotypes were significant factors affecting CRP-AUC in patients with RA receiving low-dose MTX. Based on these findings, CRP-AUC would be higher in older patients than in younger patients and, if patients had *RFC* 80AA genotypes, CRP-AUC would be higher in patients with *GGH* −401CT/TT genotypes than in those with the CC genotype.

Previous reports suggest that *RFC* G80A polymorphism is associated with altered MTX plasma level (12). Moreover Molin *et al.* suggested that patients with AA genotype of *RFC* 80 tended to have higher folate polyglutamate levels in blood cells (30). Recent evidence suggests that patients with the *RFC* 80AA genotype responded to therapy better than those with the GG and GA genotypes (13). The results of univariate analysis in our study are consistent with these reports. The *RFC* G80A·SNP causing the amino acid change (Arg to His) in the transmembrane domain was expected to alter RFC transport activity (31). Several amino acid changes in a transmembrane domain of RFC in antifolate-resistant cells were shown to change the ratio of RFC affinities to [^{3}H] MTX vs. other folate substrates (32, 33). These reports and our results suggest that the *RFC* 80A allele may potentiate the effect of low-dose MTX in patients with RA. Hence, patients with the *RFC* 80A allele and *GGH* −401CT/TT genotypes were less responsive to MTX than those without *GGH* −401T alleles in the present study.

Chave *et al.* indicated that a *GGH* C−401T polymorphism in the *GGH* promoter region was associated with increased luciferase activity and hypothesized that the polymorphism may result in increased GGH activity, followed by the

deconjugation of MTX-PGs (20). However, if GGH activity was increased by C–401T polymorphism, the anti-DHFR effect would not be increased even if the MTX concentrations in the cells were higher. Some investigators have advocated routine monitoring of MTX-PGs in red blood cells for management of RA (34–37). Dervieux *et al.* reported that there was an inverse association between *RFC* 80AA and *GGH* –401TT homozygosity and intracellular MTX-PGs concentrations (23); this finding is in good agreement with our results. In our study, 36%, 40%, and 15% of the RA patients were carriers of *RFC* 80AA, *GGH* –401CT/TT and of both *RFC* 80AA and *GGH* –401CT/TT, respectively.

There was no relationship between *GGH* C452T SNP and CRP-AUC in our study. The *GGH* C452T located in exon 5 of the *GGH* gene involving Thr to Ile amino acid exchange resulted in decreased catalytic activity of GGH (21). The allele frequency of *GGH* 452T in a Japanese population is only 5·6% (22). We speculate that there was no statistical relationship between *GGH* C452T and inflammatory status because of low allele frequency. In our study, there was no relationship between *MTHFR* SNPs and CRP-AUC, but Urano *et al.* reported that patients with RA having the MTHFR 677C-1298C haplotype received lower doses of MTX and responded better to treatment than those without it (25). Thus, MTHFR is an important enzyme in the folate metabolic pathway.

In conclusion, we found that the SNPs combination, *RFC* G80A and *GGH* C–401T, could be promising for monitoring anti-inflammatory status in MTX-treated patients with RA, and could be considered as a possible marker for drug response against MTX. Larger confirmatory prospective studies would be valuable.

ACKNOWLEDGEMENTS

We thank Dr Osamu Kimoto, Ms. Chiharu Kuroda and the professional nurses at Shizuoka Kosei Hospital for their medical expertise, and Mr Naoto Harada, University of Shizuoka for his technical support.

REFERENCES

1 Andersen PA, West SG, O'Dell JR, Via CS, Claypool RG, Kotzin BL (1985) Weekly pulse methotrexate in rheumatoid arthritis. Clinical and immunologic effects in a randomized, double-blind study. *Annals of Internal Medicine*, **103**, 489–496.

2. Evans WE, Relling MV, Rodman JH, Crom WR, Boyett JM, Pui CH (1998) Conventional compared with individualized chemotherapy for childhood acute lymphoblastic leukemia. *The New England Journal of Medicine*, **338**, 499–505.
3. Gorlick R, Goker E, Trippett T, Waltham M, Banerjee D, Bertino JR (1996) Intrinsic and acquired resistance to methotrexate in acute leukemia. *The New England Journal of Medicine*, **335**, 1041–1948.
4. Pui CH, Campana D, Evans WE (2001) Childhood acute lymphoblastic leukaemia – current status and future perspectives. *The Lancet Oncology*, **2**, 597–607
5. Pui CH, Evans WE (1998) Acute lymphoblastic leukemia. *The New England Journal of Medicine*, **339**, 605–615.
6. Weinblatt ME, Coblyn JS, Fox DA *et al.* (1985) Efficacy of low-dose methotrexate in rheumatoid arthritis. *The New England Journal of Medicine*, **312**, 818–822.
7. American College of Rheumatology Subcommittee on Rheumatoid Arthritis Guidelines. (2002) Guidelines for the management of rheumatoid arthritis: 2002 Update. *Arthritis and Rheumatism*, **46**, 328–346.
8. van Ede AE, Laan RF, Blom HJ, De Abreu RA, van de Putte LB (1998) Methotrexate in rheumatoid arthritis: an update with focus on mechanisms involved in toxicity. *Seminars in arthritis and rheumatism*, **27**, 277–292.
9. Bathon JM, Martin RW, Fleischmann RM *et al.* (2000) A comparison of etanercept and methotrexate in patients with early rheumatoid arthritis. *The New England Journal of Medicine*, **343**, 1586–1593.
10. Seideman P (1993) Methotrexate – the relationship between dose and clinical effect. *British Journal of Rheumatology*, **32**, 751–753.
11. Strand V, Cohen S, Schiff M *et al.* (1999) Treatment of active rheumatoid arthritis with leflunomide compared with placebo and methotrexate. Leflunomide Rheumatoid Arthritis Investigators Group. *Archives of Internal Medicine*, **159**, 2542–2550.
12. Laverdiere C, Chiasson S, Costea I, Moghrabi A, Krajinovic M (2002) Polymorphism G80A in the reduced folate carrier gene and its relationship to methotrexate plasma levels and outcome of childhood acute lymphoblastic leukemia. *Blood*, **100**, 3832–3834.
13. Drozdzik M, Rudas T, Pawlik A, Gornik W, Kurzawski M, Herczynska M (2007) Reduced folate carrier-1 80G>A polymorphism affects methotrexate treatment outcome in rheumatoid arthritis. *The Pharmacogenomics Journal*, **7**, 404–407
14. Goldman ID, Lichtenstein NS, Oliverio VT (1968) Carrier-mediated transport of the folic acid analogue, methotrexate, in the L1210 leukemia cell. *Journal of Biological Chemistry*, **243**, 5007–5017.

15. Shane B (1989) Folylpolyglutamate synthesis and role in the regulation of one-carbon metabolism. *Vitamins and Hormones*, **45**, 263–335.
16. Zhao R, Goldman ID (2003) Resistance to antifolates. *Oncogene*, **22**, 7431–7457.
17. Rots MG, Pieters R, Kaspers GJ, Veerman AJ, Peters GJ, Jansen G (2000) Classification of ex vivo methotrexate resistance in acute lymphoblastic and myeloid leukaemia. *British Journal of Haematology*, **110**, 791–800.
18. Panetta JC, Wall A, Pui CH, Relling MV, Evans WE (2002) Methotrexate intracellular disposition in acute lymphoblastic leukemia: a mathematical model of gamma-glutamyl hydrolase activity. *Clinical Cancer Research*, **8**, 2423–2429.
19. Rhee MS, Lindau-Shepard B, Chave KJ, Galivan J, Ryan TJ (1998) Characterization of human cellular gamma-glutamyl hydrolase. *Molecular Pharmacology*, **53**, 1040–1046.
20. Chave KJ, Ryan TJ, Chmura SE, Galivan J (2003) Identification of single nucleotide polymorphisms in the human gamma-glutamyl hydrolase gene and characterization of promoter polymorphisms. *Gene*, **319**, 167–175.
21. Cheng Q, Wu B, Kager L *et al.* (2004) A substrate specific functional polymorphism of human gamma-glutamyl hydrolase alters catalytic activity and methotrexate polyglutamate accumulation in acute lymphoblastic leukaemia cells. *Pharmacogenetics*, **14**, 557–567.
22. Hayashi H, Fujimaki C, Inoue K, Suzuki T, Itoh K (2007) Genetic polymorphism of C452T (T127I) in human gamma-glutamyl hydrolase in a Japanese population. *Biological and Pharmaceutical Bulletin*, **30**, 839–841.
23. Dervieux T, Kremer J, Lein DO *et al.* (2004) Contribution of common polymorphisms in reduced folate carrier and gamma-glutamylhydrolase to methotrexate polyglutamate levels in patients with rheumatoid arthritis. *Pharmacogenetics*, **14**, 733–739.
24. Ulrich CM, Yasui Y, Storb R *et al.* (2001) Pharmacogenetics of methotrexate: toxicity among marrow transplantation patients varies with the methylenetetrahydrofolate reductase C677T polymorphism. *Blood*, **98**, 231–234.
25. Urano W, Taniguchi A, Yamanaka H *et al.* (2002) Polymorphisms in the methylenetetrahydrofolate reductase gene were associated with both the efficacy and the toxicity of methotrexate used for the treatment of rheumatoid arthritis, as evidenced by single locus and haplotype analyses. *Pharmacogenetics*, **12**, 183–190.
26. Hassell AB, Davis MJ, Fowler PD *et al.* (1993) The relationship between serial measures of disease activity and outcome in rheumatoid arthritis. *The Quarterly Journal of Medicine*, **86**, 601–607.
27. Plant MJ, Williams AL, O'Sullivan MM, Lewis PA, Coles EC, Jessop JD (2000) Relationship between time-integrated C-reactive protein levels and radiologic progression in patients with rheumatoid arthritis. *Arthritis and Rheumatism*, **43**, 1473–1477.
28. Cockcroft DW, Gault MH (1976) Prediction of creatinine clearance from serum creatinine. *Nephron*, **16**, 31–41.
29. Souverein PC, Berard A, Van Staa TP *et al.* (2004) Use of oral glucocorticoids and risk of cardiovascular and cerebrovascular disease in a population based case-control study. *Heart*, **90**, 859–865.
30. Morin I, Devlin AM, Leclerc D *et al.* (2003) Evaluation of genetic variants in the reduced folate carrier and in glutamate carboxypeptidase II for spina bifida risk. *Molecular Genetics and Metabolism.*, **79**, 197–200.
31. Whetstine JR, Gifford AJ, Witt T *et al.* (2001) Single nucleotide polymorphisms in the human reduced folate carrier: characterization of a high-frequency G/A variant at position 80 and transport properties of the His(27) and Arg(27) carriers. *Clinical Cancer Research*, **7**, 3416–3422.
32. Drori S, Jansen G, Mauritz R, Peters GJ, Assaraf YG (2000) Clustering of mutations in the first transmembrane domain of the human reduced folate carrier in GW1843U89-resistant leukemia cells with impaired antifolate transport and augmented folate uptake. *The Journal of Biological Chemistry*, **275**, 30855–30863.
33. Jansen G, Mauritz R, Drori S *et al.* (1998) A structurally altered human reduced folate carrier with increased folic acid transport mediates a novel mechanism of antifolate resistance. *The Journal of Biological Chemistry*, **273**, 30189–30198.
34. Dervieux T, Orentas Lein D, Marcelletti J *et al.* (2003) HPLC determination of erythrocyte methotrexate polyglutamates after low-dose methotrexate therapy in patients with rheumatoid arthritis. *Clinical Chemistry*, **49**, 1632–1641.
35. Kamen BA, Takach PL, Vatev R, Caston JD (1976) A rapid, radiochemical-ligand binding assay for methotrexate. *Analytical Biochemistry*, **70**, 54–63.
36. Kamen BA, Winick N (1986) Analysis of methotrexate polyglutamate derivatives *in vivo*. *Methods in Enzymology*, **122**, 339–346.
37. Schroder H, Heinsvig EM (1985) Enzymatic assay for methotrexate in erythrocytes. *Scandinavian Journal of Clinical and Laboratory Investigation*, **45**, 657–659.
38. Yi P, Pogribny I, Jill James S (2002) Multiplex PCR for simultaneous detection of 677 C → T and 1298 A → C polymorphisms in methylenetetrahydrofolate reductase gene for population studies of cancer risk. *Cancer Letters*, **181**, 209–213.

Glycobiology vol. 19 no. 7 pp. 735–742, 2009
doi:10.1093/glycob/cwp041
Advance Access publication on March 17, 2009

Involvement of chondroitin sulfate E in the liver tumor focal formation of murine osteosarcoma cells

Basappa[2,3,8], Sengottuvelan Murugan[2,3], Kazuki N Sugahara[4,5], Chun Man Lee[4,6], Gerdy B ten Dam[7], Toin H van Kuppevelt[7], Masayuki Miyasaka[4], Shuhei Yamada[1,3], and Kazuyuki Sugahara[1,3]

[3]Graduate School of Life Science, Hokkaido University, Sapporo, Japan; [4]Laboratory of Immunodynamics, Department of Microbiology and Immunology, Osaka University, Graduate School of Medicine, Suita, Japan; [5]Vascular Mapping Center, Burnham Institute for Medical Research UCSB, University of California, Santa Barbara, CA, USA; [6]Medical Center for Translational Research, Osaka University Hospital, Suita, Japan; [7]Department of Biochemistry, Nijmegen Centre for Molecular Life Sciences, Radboud University Nijmegen Medical Centre, Nijmegen, The Netherlands; and [8]Department of Chemistry, Bangalore University, Bangalore, India

Received on December 26, 2008; revised on March 10, 2009; accepted on March 12, 2009

Cell surface heparan sulfate plays a critical role in regulating the metastatic behavior of tumor cells, whereas the role of chondroitin sulfate/dermatan sulfate (CS/DS) has been little understood in this context. Here, we characterized CS/DS chains from the murine osteosarcoma cell line LM8G7, which forms tumor nodules in liver. Structural analysis of the CS/DS chains showed a higher proportion of GlcUAβ1-3GalNAc(4,6-*O*-disulfate) (E-units) in LM8G7 (12%) than in its parental cell line LM8 (6%), which rarely forms tumors in the liver. Immunostaining with GD3G7, an antibody specific to E-units, confirmed the higher expression of the epitope in LM8G7 than LM8 cells. The tumor focal formation of LM8G7 cells in the liver in mice was effectively inhibited by the preadministration of CS-E (rich in E-unit) or the preincubation of the antibody GD3G7 with the tumor cells. CS-E or GD3G7 inhibited the adhesion of LM8G7 cells to a laminin-coated plate in vitro. In addition, the invasive ability of LM8G7 cells in vitro was also reduced by the addition of CS-E or the antibody. Further, CS-E or the antibody inhibited the proliferation of LM8G7 cells dose dependently. The binding of LM8G7 cells to VEGF in vitro was also significantly reduced by CS-E and GD3G7. Thus, the present study reveals the significance of highly sulfated CS/DS structures in the liver colonization of osteosarcoma cells and also provides a framework for the development of GAG-based anticancer molecules.

Keywords: chondroitin sulfate/glycosaminoglycan/osteosarcoma/sulfation/tumor

[1]To whom correspondence should be addressed: Tel: +81-(11)-706-9055; Fax: +81-(11)-706-9055; e-mail: tjohej@sci.hokudai.ac.jp and k-sugar@sci.hokudai.ac.jp
[2]These authors contributed equally to this work.

Introduction

The metastatic cascade consists of various interactions between tumor cells and the host cells or components of the extracellular matrix (ECM) and involves migration, adhesion, and invasion, which are mediated by cell surface molecules (Fidler 2003). Proteoglycans (PGs), a class of cell surface adhesion molecules composed of glycosaminoglycan (GAG) side chains attached to core proteins, are expressed in the ECM, and have diverse functions including roles in growth factor-binding, cell–ECM interactions, cell–cell adhesion, cell proliferation, differentiation, and tissue morphogenesis and embryogenesis (Liotta 1986; Esko and Selleck 2002). Heparan sulfate (HS) or chondroitin sulfate (CS)/dermatan sulfate (DS) side chains modulate the interaction of tumor cells with host cells and ECM components (Gallagher 1989; Iida et al. 1996) and play a critical role in regulating tumor initiation, progression, and metastasis (Sanderson 2001; Munesue et al. 2007).

The GAGs in normal tissues differ in quantity and type from those found during embryonic development and in tumors (Dietrich 1984). It has become increasingly clear that heterogeneity in the structure of HS is important in regulating disease processes including cancer (Nakanishi et al. 1992). Elevated levels of CS have also been reported in transformed cells (Lv et al. 2007). Alterations in the CS structure in tumors have been correlated with an increase in malignancy (Iida et al. 1998). In animal experiments, chondroitinase (CSase) treatment slowed the progression of cancer, leading to the suggestion that CS-PGs on the surface of cancer cells are useful therapeutic targets (Denholm et al. 2001).

In addition to ECM components, malignant cells produce a variety of soluble factors such as tumor necrosis factor-α, vascular endothelial growth factor (VEGF), and heparin-binding epidermal growth factor-like growth factor (HB-EGF), which play a major role in tumor progression (Jayne et al. 2000). Among these, VEGF and its receptors, VEGFR-1 and VEGFR-2, are more highly expressed in a metastatic model than in nonmetastatic neoplasms and directly correlate with the extent of neovascularization and degree of proliferation (Takahashi et al. 1995). Generally, it is assumed that these growth factors and other signaling proteins drive the oncogenic process through direct/indirect interactions with cell surface molecules.

Cell surface molecules such as HS regulate the signal transduction of tumor cells by interacting with various growth factors such as fibroblast growth factor-2 (FGF-2) (Mundhenke et al. 2002), VEGF (Iozzo and San Antonio 2001), and HB-EGF (Chu et al. 2005). Likewise, a rare highly sulfated GlcUAβ1-3GalNAc(4S, 6S) structure (the E-unit) in CS/DS chains, where 4S and 6S stand for 4-*O*- and 6-*O*-sulfate, respectively, plays an important role in the interaction of various functional proteins (growth factors/cytokines) (Deepa et al. 2002). In addition, the

Table I. Disaccharide composition of CS/DS chains in osteosarcoma cell lines LM8 and LM8G7[a]

Unsaturated disaccharide	LM8, pmol (mol%)	LM8G7, pmol (mol%)
ΔO: ΔHexUA-GalNAc	65.7 (64.9)	50.4 (55.8)
ΔC: ΔHexUA-GalNAc(6S)	13.0 (12.8)	7.4 (8.6)
ΔA: ΔHexUA-GalNAc(4S)	15.8 (15.8)	21.4 (23.7)
ΔD: ΔHexUA(2S)-GalNAc(6S)	N.D.[d]	N.D.
ΔB: ΔHexUA(2S)-GalNAc(4S)	N.D.	N.D.
ΔE: ΔHexUA-GalNAc(4S, 6S)	6.6 (6.5)	10.7 (11.9)
ΔT: ΔHexUA(2S)-GalNAc(4S, 6S)	N.D.	N.D.
Total[b]	101.2 (100)	90.0 (100)
S/unit[c]	0.41	0.55
Molar ratio of the total disaccharides[e]	1.12:1.00	

[a]The GAG preparation from each osteosarcoma cell line was digested with CSase ABC, and the digest was analyzed by anion-exchange HPLC after labeling with a fluorophore 2-AB as described in *Material and methods*.
[b]Amounts of disaccharides/mg of dried cells.
[c]A molar ratio of sulfate to disaccharide.
[d]N.D., not detected.
[e]A molar ratio of the total CS/DS disaccharides of the two cell lines.

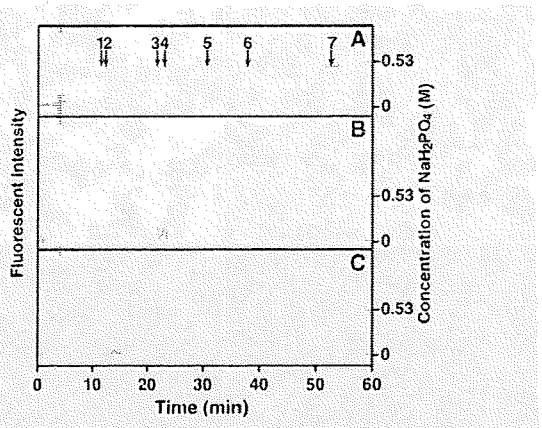

Fig. 1. Anion-exchange HPLC of CSase ABC digests of the CS/DS chains obtained from the osteosarcoma cell lines LM8 and LM8G7. The CS/DS preparations were digested individually with CSase ABC. After 2AB-labeling, each digest was analyzed by HPLC on an amine-bound silica PA-03 column using a linear gradient of NaH_2PO_4 as indicated by the dashed line. The peaks before 10 min were derived from 2AB-derivatizing reagents. (**A**) Authentic hyaluronan/CS-derived unsaturated disaccharides. (**B**) and (**C**) 2AB-labeled CS-derived unsaturated disaccharides obtained from LM8 and LM8G7 cells, respectively. Arrows indicate the elution positions of the 2AB-derivatized authentic hyaluronan and CS disaccharides: (1) $\Delta^{4,5}$HexUA-GlcNAc; (2) $\Delta^{4,5}$HexUA-GalNAc; (3) $\Delta^{4,5}$HexUA-GalNAc(6S); (4) $\Delta^{4,5}$HexUA-GalNAc(4S); (5) $\Delta^{4,5}$HexUA(2S)-GalNAc(6S); (6) $\Delta^{4,5}$HexUA-GalNAc(4S, 6S); (7) ΔHexUA(2S)-GalNAc(4S, 6S).

involvement of E-units in various biological functions such as neurite outgrowth (Sugahara and Mikami 2007), bone formation, and biomineralization has been reported (Miyazaki et al. 2008). However, the involvement of highly sulfated structures of CS/DS chains in the process of tumor formation in different organ sites is not well understood.

Recently, we reported the involvement of CS structures containing E-units in the metastasis of a Lewis lung carcinoma cell line (Li et al. 2008). An analysis of liver-specific tumor phenotypes has revealed the overexpression or specific structural changes of HS chains to be critical to the metastatic potential of melanoma cells (Tóvári et al. 1997). These findings prompted us to examine whether structural differences in the CS/DS chains of osteosarcoma cells explain the metastatic potential. In the present study, we demonstrated that the E-unit-containing structure of CS/DS chains in murine osteosarcoma LM8G7 cells is involved in the liver tumor focal formation.

Results

Comparison of CS/DS chains between LM8 and LM8G7 cells

The amount and composition of the unsaturated disaccharides produced by digestion with CSase ABC from the CS/DS polysaccharide chains, which had been extracted from LM8 and LM8G7 cells, are tabulated in Table I, and the representative anion-exchange HPLC chromatograms for the disaccharide analyses are shown in Figure 1. The amounts of CS/DS in LM8G7 and LM8 cells were comparable. Upon digestion with CSase ABC, CS/DS chains from both the cell lines yielded $\Delta^{4,5}$HexUAα1-3GalNAc (ΔO-unit), $\Delta^{4,5}$HexUAα1-3GalNAc(6S) (ΔC-unit), $\Delta^{4,5}$HexUAα1-3GalNAc(4S) (ΔA-unit), and $\Delta^{4,5}$HexUAα1-3GalNAc(4S, 6S) (ΔE-unit) in varying proportions. The degree of sulfation of CS/DS chains was relatively higher (0.55) in LM8G7 cells than in LM8 cells (0.41) (Table I). The proportion of the highly sulfated disaccharide ΔE-unit was higher in LM8G7 cells (12%) than LM8 cells (6%). The proportion of ΔC-units was significantly lower in LM8G7 cells (9%) than in LM8 cells (13%), whereas the proportion of ΔA-units was higher in LM8G7 cells (24%) than LM8 cells (16%).

In view of the recent finding of a higher proportion of E-units in the highly metastatic Lewis lung carcinoma cell line LM66-H11 than in the low metastatic cell line P29 (Li et al. 2008), it was speculated that the higher proportion of E-units in the CS/DS preparation of LM8G7 cells may be a key factor in the tumor focal formation in the liver. To confirm the overexpression of E-units on the surface of LM8G7 cells, a phage display antibody (GD3G7) specific to CS-E (Purushothaman et al. 2007; ten Dam et al. 2007; Li et al. 2008) was used for the immunostaining of the osteosarcoma cell lines. LM8G7 cells were more strongly stained by GD3G7 than were LM8 cells (Figure 2), suggesting higher levels of the expression of the E-unit.

Characterization of antitumor activity of CS isoforms

To examine the involvement of CS/DS in the liver tumor focal formation, various commercial CS preparations such as CS-A, CS-C, and CS-E (100 μg) were individually preinjected into mice 30 min before the intravenous injection of LM8G7 cells. Among the CS preparations tested, CS-E characterized by a high proportion (62%) of E-units (Kinoshita et al. 1997) completely inhibited the colonization of LM8G7 cells (Figure 3D), suggesting the importance of the E-unit in the tumor focal formation in the liver. Dose-dependent inhibition experiments showed that CS-E inhibited the tumor focal formation of LM8G7 cells strongly at 100 or 150 μg but not at all at low doses (25 or 50 μg) (Figure 4A). Heparin, a well-known antitumor agent (Borsig et al. 2001), also inhibited the liver colonization of LM8G7 cells (Figure 3G), whereas CS-A or CS-C failed to inhibit it (Figure 3B and C).

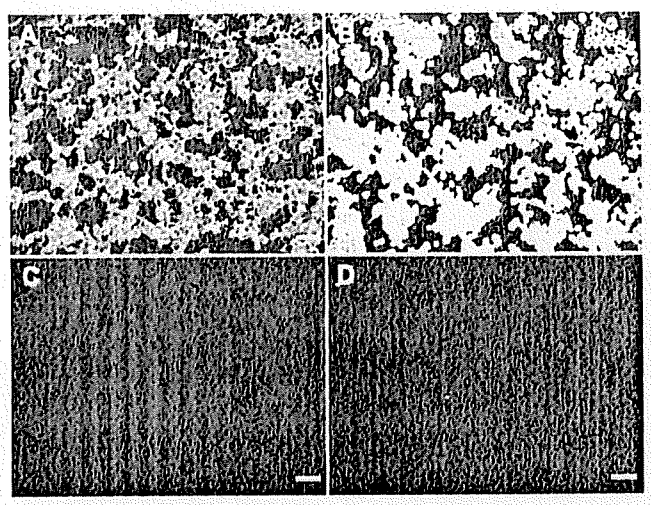

Fig. 2. Immunocytological detection of the GD3G7 epitope on the surface of murine osteosarcoma LM8 and LM8G7 cells. LM8 (**A**) and LM8G7 (**B**) cells were seeded separately on chamber slides, cultured for 24 h, and fixed with Diff-Quick reagent A. They were incubated with the antibody GD3G7 for 1 h, and bound GD3G7 was detected with an anti-VSV glycoprotein antibody followed by an Alexa-conjugated third antibody and visualized by confocal microscopy. In control experiments, LM8G7 cells were stained without GD3G7 (**C**) or irrelevant antibody MPB49V (**D**). Scale bar, 100 μm.

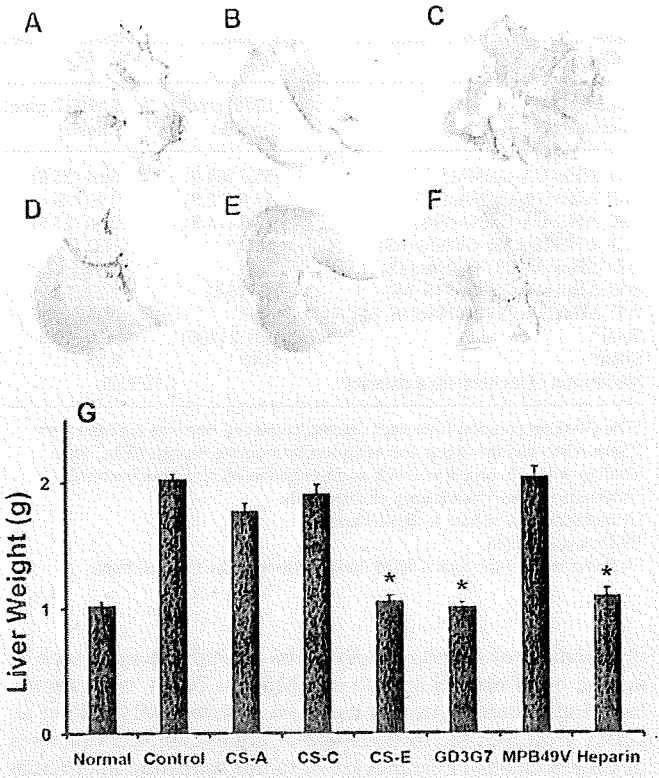

Fig. 3. Effects of CS isoforms and the antibody GD3G7 on the liver tumor focal formation of LM8G7 cells. The CS/DS preparation (100 μg) in 200 μL of Dulbecco's Modified Eagle's Medium (DMEM) was injected into a tail vein of C3H/HeN mouse 30 min before the injection of LM8G7 cells (1×10^6). LM8G7 cells were also preincubated with the antibody GD3G7 (2 μg) or the control antibody MPB49V (2 μg) for 30 min at 37°C and used for the tumor colonization experiments. Representative livers from the mice treated with DMEM (Control) (**A**), CS-A (**B**), CS-C (**C**), CS-E (**D**), antibody GD3G7 (**E**), or MPB49V (**F**) are shown. The average liver weight of the control and treated mice (**G**). Heparin from porcine intestinal mucosa (100 μg) was used as a positive control. The data represent mean values ± SD for two independent experiments. $^*P < 0.01$ versus control. Mann–Whitney *U* test.

Antitumor activity of the antibody GD3G7

The higher expression of E-units on the surface of LM8G7 cells and the strong antitumor activity of CS-E led us to hypothesize that E-unit-containing CS/DS chains on the tumor cell surface are involved in the liver tumor focal formation. It should be noted that the colonization of LM8G7 cells is specific to the liver, and no tumor colony formation was observed in other mouse organs including the lungs (data not shown). To test our hypothesis, the antibody GD3G7, which recognizes E-unit-containing CS/DS chains, was used for antitumor assays. The preincubation of LM8G7 cells with the antibody (0.2–2 μg) for 30 min strongly inhibited the liver tumor focal formation in a dose-dependent manner (Figures 3E and 4B), whereas the irrelevant antibody MPB49V (2 μg) failed to inhibit it (Figure 3F and 3G), suggesting that the epitopes for the antibody GD3G7 play a key role in the liver colonization of LM8G7 cells.

Effects of CS-E and GD3G7 on adhesion and invasion of LM8G7 cells

Effects of CS-A, CS-E (50 μg), or the antibody GD3G7 (2 μg) on the adhesion of LM8G7 cells to a laminin-coated plate were examined. Laminin, a major basement membrane protein, plays an important role in the interaction of tumor cells with the basement membrane during the extravasation step of metastasis (Baba et al. 2008). CS-E and the antibody GD3G7 inhibited the adhesion of LM8G7 cells to the substrate (Figure 5). In contrast, CS-A or the control antibody MPB49V had no effect on the attachment of LM8G7 cells to laminin.

Since the adhesion of tumor cells to basement membranes is an initial step in the invasion process, it was examined whether the antitumor effects of CS-E and GD3G7 are also due to the inhibition of cell invasion. The effects of CS-A, CS-C, CS-E (50 μg), or GD3G7 (2 μg) on the invasion by LM8G7 cells of Matrigel™ were tested. The invasive ability of the cells was reduced by CS-E and the antibody, but CS-A and CS-C had no significant effect (Figure 6). These results indicate CS-E-like epitopes to be involved in the invasion by LM8G7 cells as well.

Effects of CS-E and the antibody GD3G7 on the proliferation of LM8G7 cells

To examine the effects of GAGs and GD3G7 on cell proliferation, LM8G7 cells (5×10^3) were seeded and CS-A (100 μg), CS-C (100 μg), CS-E (50–150 μg), heparin (100 μg), or an antibody (2–5 μg) in DMEM containing 10% FBS was added. CS-E and GD3G7 inhibited the proliferation in a dose-dependent manner (Figure 7), whereas CS-A and CS-C showed no effect. Heparin, as a positive control, inhibited the proliferation of LM8G7 cells. These observations led us to conclude that CS/DS chains at the cell surface play a major role in the proliferation of tumor cells.

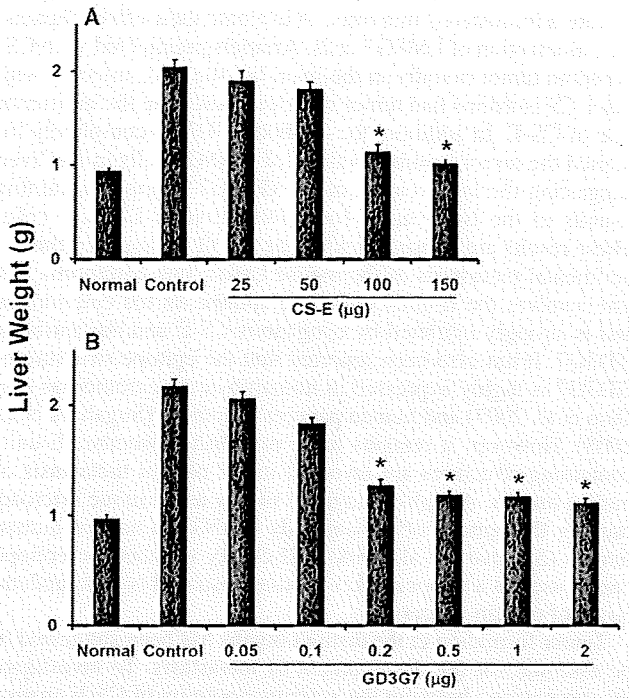

Fig. 4. Dose-dependent antitumor activity of CS-E and the antibody GD3G7. (**A**) The antitumor activity of various doses (25, 50, 100, or 150 μg) of CS-E was investigated as described in the legend to Figure 2. (**B**) LM8G7 cells were preincubated with the antibody GD3G7 at different doses (0.05, 0.1, 0.2, 0.5, 1, or 2 μg) for 30 min and used for the analysis of tumor focal formation as described in the legend to Figure 2. Six mice were used per group. The data represent mean values ± SD for two independent experiments. $^{*}P < 0.01$ versus control. Mann-Whitney *U* test.

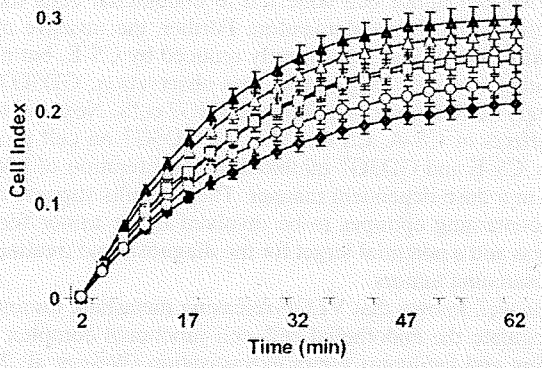

Fig. 5. Real-time monitoring of the effects of CS-A, CS-E, or GD3G7 on the adhesion of LM8G7 cells to the laminin substrate. LM8G7 cells (2×10^4) were seeded in ACEA's 96× e-plate™ coated with (Δ) or without laminin (◇), and the effects of CS-A (50 μg, ▲), CS-E (50 μg, ○), GD3G7 (2 μg, ◇), and MPB49V (2 μg, □) were observed for 60 min using the RT-CES™ system as described in *Material and methods*. The cell index (quantitative measurement of cells in a well containing an electrode) values were plotted against time. The data represent mean values ± SD for three independent experiments.

Comparison of the binding of LM8G7 cells to various growth factors

VEGF, expressed by tumor cells, facilitates the progression of cancer (Asai et al. 1998). We examined the ability of LM8G7 cells to bind growth factors in vitro. LM8G7 cells interacted well with VEGF, FGF-2, midkine (MK), and hepatocyte growth factor (HGF), but the degree of binding was the greatest with VEGF (Figure 8A). The attachment of LM8G7 cells to VEGF was strongly inhibited by the addition of CS-E or the antibody GD3G7 but not inhibited by CS-A or CS-C. Heparin, a positive control, also inhibited the attachment of LM8G7 cells to VEGF (Figure 8B).

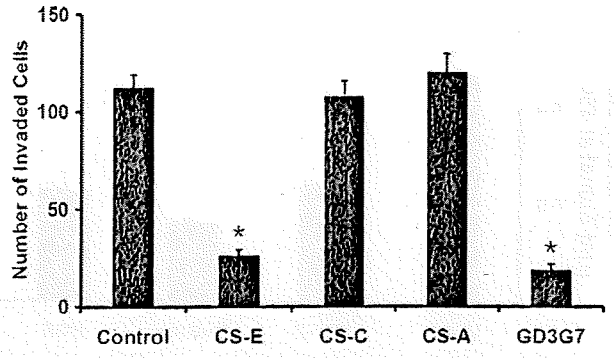

Fig. 6. Effects of various CS isoforms and the antibody GD3G7 on the invasion of LM8G7 cells. (**A**) The invasion of LM8G7 cells (2.5×10^4) was measured using a BD BioCoat™ chamber (BD Biosciences) coated with Matrigel™ in the presence or absence of CS-A, CS-C, CS-E (50 μg), or GD3G7 (2 μg) in the upper chamber and allowed to invade through the Matrigel for 24 h. The cell invasion was measured as described in *Material and methods*. The number of invaded cells is presented. The data represent mean values ± SD for two independent experiments. $^{*}P < 0.01$ versus control. Mann–Whitney *U* test.

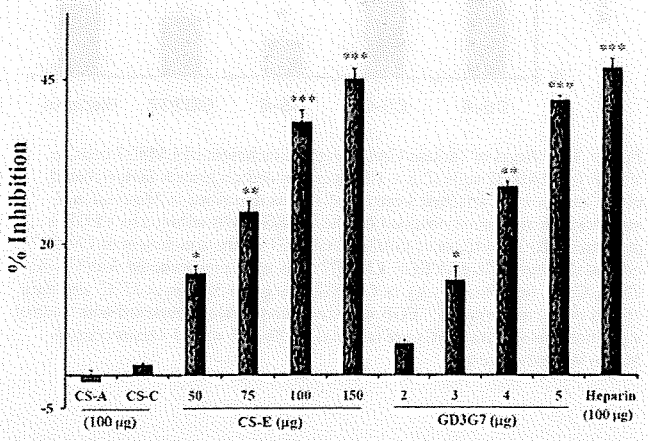

Fig. 7. Effects of various GAGs and the antibody GD3G7 on the proliferation of LM8G7 cells. (**A**) LM8G7 cells (5×10^3) were plated on 96-well plates in DMEM supplemented with 10% fetal bovine serum (FBS) in the presence or absence of CS-A (100 μg), CS-C (100 μg), CS-E (50 to 150 μg), heparin (100 μg), or the antibody GD3G7 (2 or 5 μg). The number of viable cells was determined 3 days after seeding. The data represent mean values ± SD for three independent experiments. $^{*}P < 0.01$ versus control. $^{**}P < 0.05$ versus control. Mann–Whitney *U* test.

Discussion

PGs associated with the surface of cancer cells have been recognized as important in a variety of cancers (Blackhall et al. 2001). Alterations in the level of expression of the GAG structure and/or

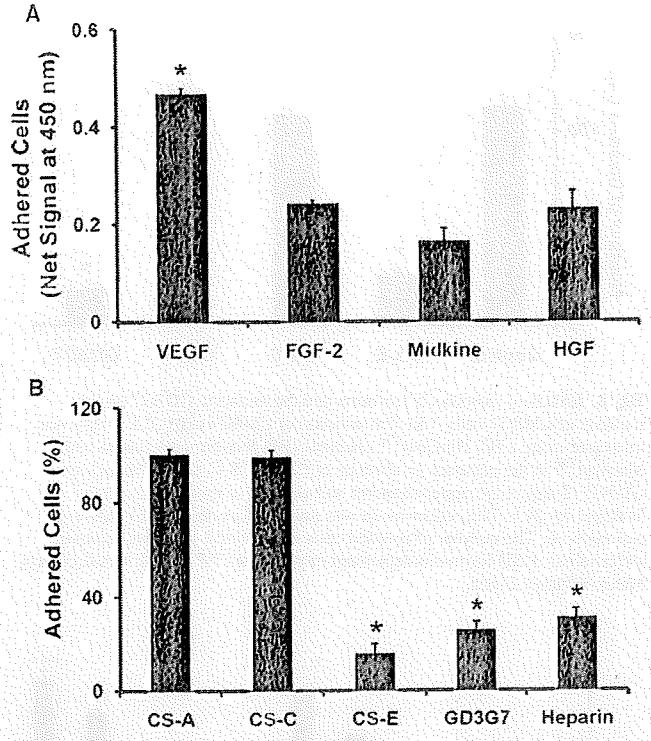

Fig. 8. The effects of various GAGs on the attachment of LM8G7 cells to VEGF. (**A**) LM8G7 cells (2.5×10^4) were seeded on growth factor-coated plates and the cells attached were quantified as described in *Material and methods*. The net signal obtained for the LM8G7 cells adhered to VEGF is presented. (**B**) The effects of GAGs or GD3G7 on the attachment of LM8G7 cells to the immobilized VEGF. LM8G7 cells were preincubated with CS-A, CS-C, CS-E, heparin (50 μg), or GD3G7 (2 μg) for 30 min at 37°C, and their effects on the adhesion of VEGF were measured. Values obtained with control wells not treated with GAGs are taken as 100%. $^*P < 0.01$ versus control. Mann–Whitney *U* test.

density on PGs can potentially make cancer cells highly versatile in modulating their behavior. For instance, significant changes in the PG content and GAG structure in tumors have been reported (Theocharis 2002). It has been demonstrated that the disaccharide composition of cell surface HS varies during the transition from human colon adenoma to carcinoma (Jayson et al. 1998). Low-sulfated HS facilitates metastasis through the adhesion of hepatoma cells to the ECM (Robinson et al. 1984). In addition, low levels of cell surface HS are correlated well with the high metastatic activity of many tumors (Redini et al. 1986; Kure et al. 1987; Sugahara et al. 1989; Timar et al. 1992).

This study revealed heterogeneous yet unique structures in the CS/DS chains of LM8 and LM8G7 cells. The major disaccharide present in LM8 and LM8G7 cells was the unsulfated unit, levels of which were lower in LM8G7 than LM8 cells. An important finding of this study was the higher proportion of E-units in the CS/DS chains of LM8G7 than LM8 cells. In addition, LM8G7 cells were more strongly immunostained by the antibody GD3G7 than were LM8 cells, supporting the increased expression of E-units in LM8G7 cells. The results of our study indicate the correlation between highly sulfated CS structures and the metastatic potential of osteosarcoma cells. To investigate the relationship between the CS-E-like-structures and the liver tumor focal formation, various CS isoforms including CS-E were administered into mice to evaluate their effects against the colonization of LM8G7 cells. Animals preinjected with CS-E had no tumor nodules in the liver, but the mice injected with other CS isoforms had tumor nodules, indicating the antitumor role of CS-E. In addition, the antibody GD3G7 completely inhibited the tumor forming activity of LM8G7 cells in the liver, suggesting the involvement of the GD3G7 epitope containing E-units in the liver tumor focal formation of LM8G7 cells. These results are consistent with our recent finding that the experimental metastasis of the mouse Lewis lung carcinoma cell line involves the E-unit-containing epitope on the cell surface and is strongly inhibited by exogenous CS-E and the antibody GD3G7. It has also been reported that the epitope structure of GD3G7 is highly expressed in human ovarian carcinomas (ten Dam et al. 2007) and human pancreatic tumors (Sugahara et al. 2008). However, it remains to be established whether E-unit-containing structures are involved in the natural metastasis of human tumors. A high-throughput survey using tissue microarrays for the epitope of the antibody GD3G7 in natural human tumors (Sugahara et al. 2008) will clarify whether the epitope can be used as a tumor marker for diagnosis and is a therapeutic target of certain cancers.

Tumor formation in the distinct organs has been suggested to be essential for the development of metastasis. To investigate the mechanistic basis for the antitumor activity of CS-E against LM8G7 cells, we performed adhesion, invasion, and proliferation experiments in vitro to validate the effects of CS isoforms on the liver tumor focal formation of LM8G7 cells. We dynamically monitored the attachment of tumor cells to the laminin-coated plate in the presence or absence of CS isoforms or the antibody GD3G7. Both CS-E and GD3G7 markedly inhibited the attachment of LM8G7 cells to the laminin-coated plate. Therefore, it is reasonable to hypothesize that the preadministration of CS-E may weaken tumor cell adhesion to endothelial cells thereby preventing the liver colonization. Further, the invasive ability of LM8G7 cells was significantly reduced by CS-E, but not by the other isoforms. Supporting this observation, GD3G7 also strongly inhibited the invasion by LM8G7 cells. Next, we tested the effects of CS-A, CS-C, CS-E, or GD3G7 on cell proliferation. CS-E and GD3G7 inhibited the proliferation of LM8G7 cells in a dose-dependent manner. These results suggest the E-unit-containing epitopes to be involved in the tumor forming process and a potential target for the diagnosis and treatment of osteosarcoma tumors.

It is well known that VEGF-releasing metastatic tumor cells dysregulate the endothelial cell–cell junctional complex upon binding and facilitates tumor extravasation (Weis et al. 2004). In this study, the addition of CS-E or GD3G7 strongly inhibited the interaction of tumor cells with VEGF. The most plausible explanation for this inhibition would be the direct binding of soluble CS-E to immobilized VEGF thereby preventing the attachment of tumor cells to VEGF, since it has been reported that highly sulfated CS-E interacts with VEGF in vitro (ten Dam et al. 2007). These results may also explain the inhibitory effects of CS-E on the liver colonization of LM8G7 cells. Thus, the present study reveals the significance of highly sulfated CS/DS structures in the liver tumor focal formation of the osteosarcoma cells and also provides a framework for the development of GAG-based anticancer molecules (Yamada and Sugahara 2008).

Material and methods

Materials

Standard unsaturated CS disaccharides, CSase ABC (EC 4.2.2.4), CS-A from whale cartilage, CS-C from shark cartilage, and CS-E from squid cartilage, and cell proliferation assay kit, TetraColor One, were purchased from Seikagaku Corp. (Tokyo, Japan). Recombinant human (rh)-HGF was from PeproTech EC Ltd (London, UK). rh-VEGF-165, rh-FGF-2, and rh-MK were obtained from Wako Pure Chemicals Co. (Osaka, Japan). The single chain antibody GD3G7 was selected for reactivity with rat embryo-derived GAGs by the phage display technique (ten Dam et al. 2007). The monoclonal anti-vesicular stomatitis virus glycoprotein (VSV-G) tag antibody P5D4 was from Sigma (St. Louis, MO). Porcine intestinal mucosal heparin was obtained from Nacalai Tesque (Kyoto, Japan). Alexa Fluor 488-conjugated goat anti-mouse IgG (H+L) was obtained from Invitrogen. Actinase E was from Kaken Pharmaceutical Co. (Tokyo, Japan). Mouse sarcoma laminin from the basement membrane of Engelbreth-Holm Swarm was obtained from Sigma. 2-Aminobenzamide (2AB) was purchased from Nacalai Tesque (Kyoto, Japan). Sodium cyanoborohydride ($NaBH_3CN$) was from Aldrich Chemical Co. (Milwaukee, WI). 100× nonessential amino acids, β-mercaptoethanol, 100× sodium pyruvate, the cell dissociation buffer, and L-glutamine were from GIBCO (Auckland, New Zealand). The Diff-Quick solution was from International Reagent Corp. (Kobe, Japan). All other chemicals and reagents were of the highest quality available.

Animals and cell lines

Nine-week-old female C3H/HeN mice were obtained from Japan SLC (Hamamatsu, Japan) and kept in standard housing. All the experiments were performed according to protocols approved by the local animal care committee of Hokkaido University. The murine osteosarcoma cell line LM8G7, which has high metastatic potential to liver, was cloned from LM8G5 cells (Lee et al. 2002) as described (Fidler and Nicolson 1976) and cultured in DMEM supplemented with 10% (v/v) FBS (Thermo Trace, Melbourne, Australia), streptomycin (100 μg/mL), penicillin (100 units/mL), 100× nonessential amino acids, β-mercaptoethanol (50 μM), 100× sodium pyruvate, and L-glutamine (2 mM) at 37°C in a humidified 5% CO_2 atmosphere. The cells were harvested after being incubated with 0.1% trypsin/1 mM EDTA in phosphate-buffered saline (PBS) for 5 min at 37°C, gently flushed with a pipette, and subcultured three times a week.

Extraction of GAGs from LM8 and LM8G7 cells

Cells were dehydrated and delipidated by extraction with acetone, air-dried, and used for the extraction of GAGs essentially as previously described (Li et al. 2007) with some modifications. Briefly, the acetone powder was digested with heat-activated (60°C, 30 min) actinase E in 200 μL of 0.1 M sodium borate, pH 8.0, containing 10 mM calcium acetate at 60°C for 48 h. After the incubation, each sample was treated with 5% trichloroacetic acid and kept for 30 min at 4°C. The precipitate was removed by centrifugation. The supernatant was extracted with diethyl ether to remove the trichloroacetic acid. After neutralization with 1.0 M sodium carbonate, the aqueous phase was adjusted to contain 80% ethanol and 1% sodium acetate, and kept at 4°C overnight. The precipitated crude GAGs were recovered by centrifugation, desalted on a PD-10 column (GE Healthcare, Buckinghamshire, UK) using the 50 mM pyridine acetate buffer, pH 5.0, as an eluent, and evaporated dry.

Analysis of the disaccharide composition of CS chains

The disaccharide composition of GAG preparations from the osteosarcoma cell lines was determined as described (Li et al. 2007). Briefly, the samples were dissolved in water, and an aliquot was digested with CSase ABC (Saito et al. 1968) and labeled with 2AB (Kinoshita and Sugahara 1999). The excess 2AB was removed by extraction with chloroform (Kawashima et al. 2002). The 2AB-labeled digest was analyzed by anion-exchange HPLC on a PA-03 silica column (YMC-Pack PA, Kyoto, Japan) with a linear gradient of NaH_2PO_4 from 16 to 538 mM over 60 min at a flow rate of 1.0 mL/min at room temperature. Identification and quantification of the resulting disaccharides were achieved by comparison with the elution of authentic CS-derived unsaturated disaccharides (Kinoshita and Sugahara 1999).

Immunocytochemistry

To detect the E-unit-containing epitopes, murine osteosarcoma cell lines, LM8 and LM8G7, were stained using a phage display single chain antibody, GD3G7 (Purushothaman et al. 2007; ten Dam et al. 2007). Briefly, osteosarcoma cells were plated on 8-well Lab-Tech chamber slides (Nalge Nunc International, Roskilde, Denmark), cultured for 24 h, and fixed with Diff-Quick reagent A. After being blocked with PBS containing 3% bovine serum albumin (BSA) for 1 h at room temperature, the fixed cells were incubated with 100 μL of the primary antibody GD3G7 (diluted 1:100 (10 μg/mL) in 0.1% BSA/PBS) for 1 h at room temperature and washed with PBS. After being incubated with the anti-VSV-G antibody (diluted 1:5,000 in 0.1% BSA/PBS) for 1 h at room temperature, the cells were washed with PBS. To detect the anti-VSV-G antibody, the cells were stained with a third antibody conjugated to Alexa Fluor 488 (diluted 1:5000 in 0.1% BSA/PBS) and visualized with a laser-scanning confocal microscope, FLUOVIEW (Olympus, Tokyo, Japan).

Assay of liver tumor focal formation

In preparation for injection, LM8G7 cells were harvested after a brief exposure to a cell dissociation buffer (GIBCO) and the cell viability in single-cell suspensions was determined by trypan blue exclusion. A total of 1×10^6 cells suspended in 200 μL of DMEM were injected into a lateral tail vein of C3H/HeN mice. Four weeks later, the animals were sacrificed. The number of visible tumor cell nodules in the liver was examined and liver weight was recorded.

To elucidate the involvement of cell surface CS/DS in the liver tumor focal formation, the C3H/HeN mice received 100 μg of commercial CS preparations (CS-A, CS-C, or CS-E) or heparin 30 min before the tumor cell injection. The dose-dependent inhibition experiments were carried out using CS-E (25, 50, 100, or 150 μg). In other instances, to investigate the involvement of the antibody GD3G7 epitope in the liver tumor focal formation, LM8G7 cells were preincubated with serially diluted GD3G7 (0.05, 0.1, 0.2, 0.5, 1, or 2 μg) or the irrelevant antibody MPB49V (2 μg) for 30 min at 37°C. Aliquots of the cell

suspension were assessed for cell viability before the injection. After incubated with antibodies (GD3G7 or MPB49V) and prior to the injection of the tumor cells into animals, it was ensured by microscopic observations that these cells were in a single cell suspension.

Real-time monitoring of the adhesion of LM8G7 cells to the laminin substrate

The cell attachment assay was carried out using the RT-CES™ system (ACEA Biosciences, San Diego, CA). ACEA's 96× microtiter plates were coated with laminin (0.5 μg/well) at 37°C for 1 h. Attachment and spreading of LM8G7 cells (2×10^4) were monitored in the presence or absence of various inhibitors such as CS-A (50 μg), CS-E (50 μg), the antibody GD3G7 (2 μg), or the control antibody MPB49V (2 μg), and continuously monitored for up to 62 min using the RT-CES™ system. The cell index (quantitative measurement of cells in a well containing an electrode) was plotted against time.

Cell invasion assay in vitro

The invasion of LM8G7 cells across the Matrigel™-coated porous membranes was assessed using a 24-well plate (8 μm pore size, insert size: 6.4 μm) (BD Biosciences, Franklin Lakes, NJ) according to the manufacturer's protocol. Briefly, single cell suspensions of LM8G7 cells (2.5×10^4) were prepared by detaching and resuspending the cells in DMEM containing 0.1% BSA. Before the cells were added, the chambers were rehydrated for 2 h in an incubator at 37°C. The lower chambers were filled with DMEM containing 5% FBS. In some instances, LM8G7 cells (2.5×10^4) in serum-free DMEM were preincubated with CS-A, CS-C, CS-E (50 μg), or the antibody GD3G7 (2 μg) for 30 min at 37°C in a CO_2 incubator and added to the upper chamber. After incubation for 24 h, cells that had passed through the Matrigel-coated membrane and remained attached to the opposite surface of the membrane were stained with the Diff-Quick solution and counted in five random microscopic fields per filter.

Assay of cell proliferation in vitro

To examine the effects of CS isoforms on proliferation in vitro, LM8G7 cells were seeded at a density of 5×10^3 cells/well in a 96-well plate and treated with CS-E (50–150 μg), GD3G7 (2–5 μg), CS-A (100 μg), CS-C (100 μg), or heparin (100 μg) for 3 days. After a specific period of time, 5 μL of TetraColor One (Tanaka et al. 2002) reagent was added and incubated for an additional 4 h, and the absorbance at 450 nm (Bio-Rad, Hercules, CA) was measured. The viability of the cells was expressed in percentage terms.

Tumor cell-growth factor adhesion assay

The adhesion of tumor cells to various growth factors (Hibino et al. 2005) in vitro was assessed in a 96-well plate. VEGF, FGF-2, MK, and HGF (100 ng) were added to the microtiter plate and incubated overnight at 4°C. After blocking the wells with 1% BSA in PBS, DMEM-containing LM8G7 cells (2.5×10^4) in 0.1% BSA were added to a plate and incubated for 1 h at 37°C in a humidified 5% CO_2 atmosphere. After a brief wash with PBS, 100 μL of PBS containing 5 μL of TetraColor One was added and the plate was incubated for 45 min. The viable adhered cells were quantified by measuring the absorbance at 450 nm. The net signal is obtained by subtracting the background obtained with a BSA-coated well. In other instances, the cells were preincubated with CS-A, CS-C, CS-E, heparin (50 μg), or GD3G7 (2 μg) for 30 min at 37°C and used for the experiment.

Acknowledgement

Basappa and Sengottuvelan Murugan are grateful to the Japan Society for the Promotion of Science (JSPS) for a postdoctoral fellowship.

Funding

The Ministry of Education, Culture, Sports, Science, and Technology of Japan (MEXT) (20390019), the New Energy and Industrial Technology Development Organization (NEDO) (to K.S.), the Human Frontier Science Program (RGP62/2004 to T.H.v.K.), the Dutch Cancer Society, grant number 2008-4058 (to G.t.D.).

Conflict of interest statement

None declared.

Abbreviations

$\Delta^{4,5}$HexUA, 4,5-unsaturated hexuronic acid; 2AB, 2-aminobenzamide; 4S, 4-*O*-sulfate; 6S, 6-*O*-sulfate; BSA, bovine serum albumin; CS, chondroitin sulfate; DMEM, Dulbecco's modified Eagle's medium; DS, dermatan sulfate; ECM, extracellular matrix; E-unit, GlcUAβ1-3GalNAc(4S, 6S); FBS, fetal bovine serum; FGF-2, fibroblast growth factor-2; GAG, glycosaminoglycan; GalNAc, *N*-acetyl-D-galactosamine; GlcUA, D-glucuronic acid; HB-EGF, heparin-binding epidermal growth factor-like growth factor; HexUA, hexuronic acid; HGF, hepatocyte growth factor; HS, heparan sulfate; MK, midkine; PBS, phosphate-buffered saline; VEGF, vascular endothelial growth factor.

References

Asai T, Ueda T, Itoh K, Yoshioka K, Aoki Y, Mori S, Yoshikawa H. 1998. Establishment and characterization of a murine osteosarcoma cell line (LM8) with high metastatic potential to the lung. *Int J Cancer.* 76:418–422.

Baba Y, Iyama KI, Hirashima K, Nagai Y, Yoshida N, Hayashi N, Miyanari N, Baba H. 2008. Laminin-332 promotes the invasion of oesophageal squamous cell carcinoma via PI3K activation. *Br J Cancer.* 98:974–980.

Blackhall FH, Merry CL, Davies EJ, Jayson GC. 2001. Heparan sulfate proteoglycans and cancer. *Br J Cancer.* 19:1094–1098.

Borsig L, Wong R, Feramisco J, Nadeau DR, Varki NM, Varki A. 2001. Heparin and cancer revisited: Mechanistic connections involving platelets, P-selectin, carcinoma mucins, and tumor metastasis. *Proc Natl Acad Sci USA.* 98:3352–3357.

Chu CL, Goerges AL, Nugent MA. 2005. Identification of common and specific growth factor binding sites in heparan sulfate proteoglycans. *Biochemistry.* 44:12203–12213.

Deepa SS, Umehara Y, Higashiyama S, Itoh N, Sugahara K. 2002. Specific molecular interactions of oversulfated chondroitin sulfate E with various heparin-binding growth factors. Implications as a physiological binding partner in the brain and other tissues. *J Biol Chem.* 277:43707–43716.

Denholm EM, Lin YQ, Silver PJ. 2001. Anti-tumor activities of chondroitinase AC and chondroitinase B: Inhibition of angiogenesis, proliferation and invasion. *Eur J Pharmacol.* 416:213–221.

Dietrich CP. 1984. A model for cell–cell recognition and control of cell growth mediated by sulfated glycosaminoglycans. *Braz J Med Biol Res.* 17:5–15.

Esko JD, Selleck SB. 2002. Order out of chaos: Assembly of ligand binding sites in heparan sulfate. *Annu Rev Biochem.* 71:435–471.

Fidler IJ. 2003. The pathogenesis of cancer metastasis: The "seed and soil" hypothesis revisited. *Nat Rev Cancer.* 3:453–458.

Fidler IJ, Nicolson GL. 1976. Organ selectivity for implantation survival and growth of B16 melanoma variant tumor lines. *J Natl Cancer Inst.* 57:1199–11202.

Gallagher JT. 1989. The extended family of proteoglycans: Social residents of the pericellular zone. *Curr Opin Cell Biol.* 1:1201–1218.

Hibino S, Shibuya M, Hoffman MP, Engbring JA, Hossain R, Mochizuki M, Kudoh S, Nomizu M, Kleinman HK. 2005. Laminin alpha5 chain metastasis- and angiogenesis-inhibiting peptide blocks fibroblast growth factor 2 activity by binding to the heparan sulfate chains of CD44. *Cancer Res.* 65:10494–10501.

Iida J, Meijne AM, Knutson JR, Furcht LT, McCarthy JB. 1996. Cell surface chondroitin sulfate proteoglycans in tumor cell adhesion, motility and invasion. *Semin Cancer Biol.* 7:155–162.

Iida J, Meijne AM, Oegema TR Jr, Yednock TA, Kovach NL, Furcht LT, McCarthy JB. 1998. A role of chondroitin sulfate glycosaminoglycan binding site in alpha4beta1 integrin-mediated melanoma cell adhesion. *J Biol Chem.* 273:5955–5962.

Iozzo RV. 1998. Matrix proteoglycans: From molecular design to cellular function. *Annu Rev Biochem.* 67:609–652.

Iozzo RV, San Antonio JD. 2001. Heparan sulfate proteoglycans: Heavy hitters in the angiogenesis arena. *J Clin Invest.* 108:349–355.

Jayne DG, Perry SL, Morrison E, Farmery SM, Guillou PJ. 2000. Activated mesothelial cells produce heparin-binding growth factors: Implications for tumour metastases. *Br J Cancer.* 82:1233–1238.

Jayson GC, Lyon M, Paraskeva C, Turnbull JE, Deakin JA, Gallagher JT. 1998. Heparan sulfate undergoes specific structural changes during the progression from human colon adenoma to carcinoma in vitro. *J Biol Chem.* 273:51–57.

Kawashima H, Atarashi K, Hirose M, Hirose J, Yamada S, Sugahara K, Miyasaka M. 2002. Oversulfated chondroitin/dermatan sulfates containing GlcAbeta1/IdoAalpha1-3GalNAc(4,6-*O*-disulfate) interact with L- and P-selectin and chemokines. *J Biol Chem.* 277:12921–12930.

Kinoshita A, Sugahara K. 1999. Microanalysis of glycosaminoglycan-derived oligosaccharides labeled with a fluorophore 2-aminobenzamide by high-performance liquid chromatography: Application to disaccharide composition analysis and exosequencing of oligosaccharides. *Anal Biochem.* 269:367–378.

Kinoshita A, Yamada S, Haslam SM, Morris HR, Dell A, Sugahara K. 1997. Novel tetrasaccharides isolated from squid cartilage chondroitin sulfate E contain unusual sulfated disaccharide units GlcA(3-*O*-sulfate)beta1-3GalNAc(6-*O*-sulfate) or GlcA(3-*O*-sulfate)beta1-3GalNAc. *J Biol Chem.* 272:19656–19665.

Kure S, Yoshie O, Aso H. 1987. Metastatic potential of murine B16 melanoma correlates with reduced surface heparan sulfate glycosaminoglycan. *Jpn J Cancer Res.* 78:1238–1245.

Lee CM, Tanaka T, Murai T, Kondo M, Kimura J, Su W, Kitagawa T, Ito T, Matsuda H, Miyasaka M. 2002. Novel chondroitin sulfate-binding cationic liposomes loaded with cisplatin efficiently suppress the local growth and liver metastasis of tumor cells in vivo. *Cancer Res.* 62:4282–4288.

Li F, Shetty AK, Sugahara K. 2007. Neuritogenic activity of chondroitin/dermatan sulfate hybrid chains of embryonic pig brain and their mimicry from shark liver. Involvement of the pleiotrophin and hepatocyte growth factor signaling pathways. *J Biol Chem.* 282:2956–2966.

Li F, ten Dam GB, Murugan S, Yamada S, Hashiguchi T, Mizumoto S, Oguri K, Okayama M, van Kuppevelt TH, Sugahara K. 2008. Involvement of highly sulfated chondroitin sulfate in the metastasis of the Lewis lung carcinoma cells. *J Biol Chem.* 283:34294–34304.

Liotta LA. 1986. Tumor invasion and metastases – Role of the extracellular matrix. *Cancer Res.* 46:1–7.

Lv H, Yu G, Sun L, Zhang Z, Zhao X, Chai W. 2007. Elevate level of glycosaminoglycans and altered sulfation pattern of chondroitin sulfate are associated with differentiation status and histological type of human primary hepatic carcinoma. *Oncology.* 72:347–356.

Miyazaki T, Miyauchi S, Tawada A, Anada T, Matsuzaka S, Suzuki O. 2008. Oversulfated chondroitin sulfate-E binds to BMP-4 and enhances osteoblast differentiation. *J Cell Physiol.* 217:769–777.

Mundhenke C, Meyer K, Drew S, Friedl A. 2002. Heparan sulfate proteoglycans as regulators of fibroblast growth factor-2 receptor binding in breast carcinomas. *Am J Pathol.* 160:185–194.

Munesue S, Yoshitomi Y, Kusano Y, Koyama Y, Nishiyama A, Nakanishi H, Miyazaki K, Ishimaru T, Miyaura S, Okayama M, et al. 2007. A novel function of syndecan-2, suppression of matrix metalloproteinase-2 activation, which causes suppression of metastasis. *J Biol Chem.* 282:28164–28174.

Nakanishi H, Oguri K, Yoshida K, Itano N, Takenaga K, Kazama T, Yoshida A, Okayama M. 1992. Structural differences between heparan sulphates of proteoglycan involved in the formation of basement membranes in vivo by Lewis-lung-carcinoma-de[illegible]d cloned cells with different metastatic potentials. *Biochem J.* 288:215–224.

Purushothaman A, Fukuda J, Mizumoto S, ten Dam GB, van Kuppevelt TH, Kitagawa H, Mikami T, Sugahara K. 2007. Functions of chondroitin sulfate/dermatan sulfate chains in brain development. Critical roles of E and iE disaccharide units recognized by a single chain antibody GD3G7. *J Biol Chem.* 282:19442–19452.

Redini F, Moczar E, Poupon MF. 1986. Cell surface glycosaminoglycans of rat rhabdomyosarcoma lines with different metastatic potentials and of non-malignant rat myoblasts. *Biochim Biophys Acta.* 883:98–105.

Robinson J, Viti M, Höök M. 1984. Structure and properties of an under-sulfated heparan sulfate proteoglycan synthesized by a rat hepatoma cell line. *J Cell Biol.* 98:946–953.

Saito H, Yamagata T, Suzuki S. 1968. Enzymatic methods for the determination of small quantities of isomeric chondroitin sulfates. *J Biol Chem.* 243:1536–1542.

Sanderson RD. 2001. Heparan sulfate proteoglycans in invasion and metastasis. *Semin Cell Dev Biol.* 12:89–98.

Sugahara K, Mikami T. 2007. Chondroitin/dermatan sulfate in the central nervous system. *Curr Opin Struct Biol.* 17:5[illegible]545.

Sugahara K, Okumura Y, Yamashina I. 1989. The Engelbreth-Holm-Swarm mouse tumor produces undersulfated heparan sulfate and [illegible]sulfated galactosaminoglycans. *Biochem Biophys Res Commun.* 162:189–197.

Sugahara KN, Hirata T, Tanaka T, Ogino S, Takeda M, Terasawa H, Shimada I, Tamura J, ten Dam GB, van Kuppevelt TH, et al. 2008. Chondroitin sulfate E fragments enhance CD44 cleavage and CD44-dependent motility in tumor cells. *Cancer Res.* 68:7191–7199.

Takahashi Y, Kitadai Y, Bucana CD, Cleary KR, Ellis LM. 1995. Expression of vascular endothelial growth factor and its receptor, KDR, correlates with vascularity, metastasis, and proliferation of human colon cancer. *Cancer Res.* 55:3964–3968.

Tanaka Y, Nakayamada S, Fujimoto H, Okada Y, Umehara H, Kataoka T, Minami Y. 2002. H-Ras/mitogen-activated protein kinase pathway inhibits integrin-mediated adhesion and induces apoptosis in osteoblasts. *J Biol Chem.* 277:21446–21452.

ten Dam GB, van de Westerlo EM, Purushothaman A, Stan RV, Bulten J, Sweep FC, Massuger LF, Sugahara K, van Kuppevelt TH. 2007. Antibody GD3G7 selected against embryonic glycosaminoglycans defines chondroitin sulfate-E domains highly up-regulated in ovarian cancer and involved in vascular endothelial growth factor binding. *Am J Pathol.* 171:1324–1333.

Theocharis AD. 2002. Human colon adenocarcinoma is associated with specific post-translational modifications of versican and decorin. *Biochim Biophys Acta.* 1588:165–172.

Timar J, Ladanyi A, Lapis K, Moczar M. 1992. Differential expression of proteoglycans on the surface of human melanoma cells characterized by altered experimental metastatic potential. *Am J Pathol.* 141:467–474.

Tóvári J, Paku S, Rásó E, Pogány G, Kovalszky I, Ladányi A, Lapis K, Tímár J. 1997. Role of sinusoidal heparan sulfate proteoglycan in liver metastasis formation. *Int J Cancer.* 71:825–831.

Weis S, Cui J, Barnes L, Cheresh D. 2004. Endothelial barrier disruption by VEGF-mediated Src activity potentiates tumor cell extravasation and metastasis. *J Cell Biol.* 167:223–229.

Yamada S, Sugahara K. 2008. Potential therapeutic application of chondroitin sulfate/dermatan sulfate. *Curr Drug Discov Technol.* 5:289–301.

Int. J. Cancer: 125, 2316–2322 (2009)

Enhanced expression of Annexin A4 in clear cell carcinoma of the ovary and its association with chemoresistance to carboplatin

Ayako Kim[1,2], Takayuki Enomoto[1], Satoshi Serada[2], Yutaka Ueda[1], Tsuyoshi Takahashi[2,3], Barry Ripley[2], Takashi Miyatake[1], Masami Fujita[1], Chun Man Lee[4], Koji Morimoto[5], Minoru Fujimoto[2], Tadashi Kimura[1] and Tetsuji Naka[2]*

[1]*Department of Obstetrics and Gynaecology, Osaka University Graduate School of Medicine, Osaka, Japan*
[2]*Laboratory for Immune Signal, National Institute of Biomedical Innovation, Osaka, Japan*
[3]*Department of Surgery, Osaka University Graduate School of Medicine, Osaka, Japan*
[4]*Medical Center for Translational Research, Osaka University Hospital, Osaka, Japan*
[5]*Department of Breast and Endocrine Surgery, Osaka University Graduate School of Medicine, Osaka, Japan*

Clear cell carcinoma (CCC) of the ovary is known to be highly resistant to platinum-based chemotherapy. The purpose of our study was to identify a candidate protein that is associated with chemoresistance of CCC and to investigate the specific mechanism of chemoresistance conferred by the identified protein. Enhanced expression of Annexin A4 (Anx A4) was identified in ovarian CCC cells using 2-D differential gel electrophoresis (2D-DIGE) and mass spectrometry. Anx A4 levels were elevated in CCC cells compared with non-CCC cells as determined by real-time RT-PCR and Western blot analysis. Immunohistochemical analysis of Anx A4 was performed in 126 epithelial ovarian cancer tissue samples and demonstrated significantly elevated levels of Anx A4 protein levels in ovarian CCC tumors compared with ovarian serous and endometrioid tumors ($p < 0.01$). Anx A4-transfected ovarian non-CCC cells were more resistant to carboplatin (IC50 = 42 μM) compared with control cells (IC50 = 23 μM) as determined by modified MTT assay. Intracellular platinum levels were significantly lower in Anx A4-transfected cells compared with control cells after carboplatin treatment ($p = 0.0020$) and after an additional 360 min of carboplatin-free incubation ($p = 0.0004$), as measured by atomic absorption spectrophotometry. Expression of Anx A4 is elevated in ovarian CCC tumors and is associated with chemoresistance in cultured ovarian cancer cells. These results demonstrate that Anx A4 confers chemoresistance in ovarian cancer cells in part by enhancing drug efflux. Thus, Anx A4 may represent a novel therapeutic target of chemoresistance in patients with ovarian CCC.

Key words: clear cell carcinoma of the ovary; chemoresistance; Annexin A4

Ovarian cancer is the 5th leading cause of cancer deaths for women in the United States, with approximately 21,600 new cases and 15,500 deaths reported annually.[1] In Japan, it is the eighth most common cause of cancer deaths, with approximately 7,700 new cases (2001) and 4,500 deaths (2007) reported yearly, and the incidence is increasing (Health, Labour and Welfare Ministry, Japan: Population Survey Report). More than 20% of all cases with ovarian cancer in Japan are classified as clear cell carcinoma (CCC) of the ovary, and for unknown reasons, this percentage is markedly higher (by approximately 2-fold) than in Europe and the United States.[2]

Because ovarian cancers (including ovarian CCC) are relatively asymptomatic at early stage, the majority of patients (approximately 70%) present with an advanced stage disease at first diagnosis and subsequently require surgical tumor reduction and adjuvant chemotherapy.[3,4] However, of the 4 major histological types of epithelial ovarian cancer, CCC of the ovary is highly resistant to conventional cancer chemotherapy (including carboplatin and paclitaxel treatment) compared with the other histological types.[2,5,6] Consequently, patients with ovarian CCC are associated with both poorer prognosis and higher mortality than patients with other types of ovarian cancer.[2] Thus, there is an urgent need to further our understanding of the pathogenesis of ovarian CCC, particularly with respect to the expression of proteins, which confer chemoresistance, for the development of a novel therapeutic strategy.

In this study, we performed a proteomic analysis using ovarian cancer cell lines [CCC for comparison with non-CCC serous adenocarcinoma (SAC)] to identify a candidate protein associated with chemoresistance in ovarian CCC. SAC was chosen as a control non-CCC cell line because of its chemosensitivity compared with the chemoresistant CCC cell line. We identified several proteins that are differentially upregulated in ovarian CCC compared with SAC and focused our investigation on Annexin A4 (Anx A4).

Anx A4 is an epithelial isoform of a ubiquitous family of soluble cytoplasmic proteins, which bind to and polymerize on the surface of cell membranes in response to increases in intracellular calcium.[7–9] Although the functions of Anx A4 have not been completely characterized, previous studies have identified major involvement of this protein in membrane permeability,[10] exocytosis[11,12] and regulation of ion channels.[13] Its roles in membrane fluidity and membrane trafficking may in part explain the involvement of Anx A4 in modulating drug resistance in cancer cells.

A previous report associating Anx A4 with chemoresistance in human cancer cell lines focused on human lung and colon cancer cell lines[14] but did not examine ovarian cancer cell lines. In addition, the mechanism of chemoresistance induced by Anx A4 has not been explored in detail. In the study of Morita *et al.*,[15] proteomic analysis showed enhanced expression of Anx A4 in the OVISE and OVTOKO ovarian CCC cell lines compared with the MCAS ovarian mucinous cancer cell line. However, a possible association between Anx A4 expression and chemoresistance was not investigated. Importantly, neither study tried to determine whether Anx A4 protein levels are elevated in tumors of patients with ovarian CCC.

In this study, we have addressed 2 important questions concerning Anx A4 and chemoresistance, *i.e.*, whether expression of Anx A4 is elevated in patient ovarian CCC tumors and by what mechanism Anx A4 confers chemoresistance.

Material and methods

Patients

We examined surgically obtained tumor tissue samples of 126 ovarian cancer patients (Table I) who underwent surgery at Osaka University Hospital, Japan, between 1999 and 2006. None of the patients entered in this study had received adjuvant chemotherapy, including paclitaxel or carboplatin treatment. Histologic features of the tissues were reviewed by board-certified pathologists. Diagnosis was based on the FIGO (International Federation of Gynecologists &

Grant sponsor: Japanese Ministry of Education, Science, Culture and Sports (Grants-Aids for Scientific Research).
***Correspondence to:** Laboratory for Immune Signal, National Institute of Biomedical Innovation, 7-6-8 Saito-asagi, Ibaraki, Osaka 567-0085, Japan. Fax: +81-72-641-9837. E-mail: tnaka@nibio.go.jp
Received 13 February 2009; Accepted after revision 12 May 2009
DOI 10.1002/ijc.24587
Published online 20 May 2009 in Wiley InterScience (www.interscience.wiley.com).

TABLE 1 – SUMMARY OF CLINICAL CHARACTERISTICS OF OVARIAN CANCER PATIENTS EXAMINED IN THIS STUDY

Histology	Mean age (range)	FIGO stages				Total
		I	II	III	IV	
CCC	53 (36–66)	27	5	9	2	43
Endometrioid	53 (28–66)	2	7	4	0	13
Mucinous	53 (28–90)	6	1	1	0	8
SAC	55 (33–81)	9	13	35	5	62
						126

Obstetricians) classification system. Patient profiles (age, FIGO stage) were analyzed against each of the 4 major epithelial ovarian cancer histological types (CCC, endometrioid adenocarcinoma, mucinous adenocarcinoma and serous adenocarcinoma). Written informed consent was obtained for all the cases, and the experimental protocol was approved by the ethics committee of Osaka University.

Cell lines

Human clear cell carcinoma (CCC) ovarian cancer cell lines (OVISE, OVTOKO, OVMANA and RMG-1) and serous adenocarcinoma (SAC) ovarian cancer cell lines (OVSAHO and OVKATE) were obtained from the Japanese Collection of Research Bioresources (JCRB, Osaka, Japan). Cells were maintained in RPMI 1640 medium supplemented with 10% fetal bovine serum (FBS) (HyClone Laboratories, Logan, UT) and 1% penicillin–streptomycin (Nacalai Tesque, Kyoto, Japan) at 37°C under a humidified atmosphere of 5% CO_2.

Protein extraction and 2D-DIGE

Proteins extracts of the cell lines were prepared with the Complete Mammalian Proteome Extraction Kit (Calbiochem, La Jolla, CA) and stored at −80°C until use. Protein concentrations were determined with the RC-DC Protein Assay kit (Bio-Rad Laboratories, Hercules, CA) using BSA as the standard. Before 2D-DIGE, we performed fluorescence labeling, for which the OVISE and OVSAHO samples were labeled with Cy3 and Cy5 CyDye DIGE fluorminimal dyes (GE Healthcare Bio-Sciences, Little Chalfont, Buckinghamshire, UK), respectively. For first-dimension separation, isoelectric focusing electrophoresis was performed using ReadyStrip™ (Bio-Rad Laboratories) IPG strips (24 cm, pH3-10NL). The labeled proteins (150 μg) were then loaded onto a gel strip, which was rehydrated in the dark for 12 hr (99,000 Vh) with the labeled protein sample diluted to 430 μl with a rehydration buffer (7 M urea, 2 M thiourea, 4% CHAPS, 2 mM TBP, 0.0002% BPB, 1.0% Bio-lyte 3-10 and 1.2% destreak). After isoelectric focusing, proteins were reduced in an equilibration buffer (50 mM Tris-HCl containing 6 M urea, 20% v/v glycerol and 2% SDS, pH 8.8) containing 20 mg/ml DTT for 40 min followed by carbamidomethylation in the equilibration buffer containing 25 mg/ml iodoacetamide for 30 min in the dark. The second-dimension separation was performed on 10% polyacrylamide gels using the Ettan-Dalt-Six system (GE Healthcare Bio-Sciences) at a constant wattage of 100 W at 20°C for 3 hr. Gel electrophoresis was performed in the dark, and the gels were scanned with the Typhoon scanner (GE Healthcare Bio-Sciences).

Protein identification by mass spectrometry

2D-PAGE was performed in parallel with 2D-DIGE using OVISE and OVSAHO protein extracts without fluorescence labeling. Gels were stained using a Silver Stain MS Kit (WAKO Pure Chemical Industries, Ltd., Osaka, Japan). Protein spots in a silver-stained gel, corresponding to the spots of interest in the 2D-DIGE scanned image, were digested in gel according to a previously described method,[16] using sequencing grade modified trypsin (Promega, Inc., Madison, WI). Digested peptides were then extracted with 5% TFA in acetonitrile (ACN/DW 50:45), sonicated for 5 min and concentrated by evaporation. The peptides were solubilized with 0.1% TFA in ACN/DW (2:98) and analyzed by means of LC-MS/MS. For reverse-phase separations, a Magic 2002 capillary HPLC (Michrom BioResources, Auburn, CA) with a C-18 RP column (length 15 cm, i.d. 200 μm; GL Sciences Inc., Tokyo, Japan) was used. The injected peptides were then eluted with a 30-min linear gradient of 5–65% of solvent B (solvent A: 0.1% formic acid in ACN/DW, 2:98; solvent B: 0.1% formic acid in ACN/DW, 95:5). The column was directly interfaced to an LCQ ion trap mass spectrometer (ThermoElectron, San Jose, CA) equipped with a nanoelectrospray ion source, and data were collected in the double mode that was configured to alternate between a single full MS scan and an MS/MS scan of the most intense precursor masses. MS/MS spectra were searched against the human protein Swiss-Prot database with the aid of the MASCOT search program (version 2.1.03; Matrix Science K.K., Tokyo, Japan). The following parameters were used for the search: enzyme: trypsin, missed cleavage: 1, variable modification; oxidation of methionines, fixed modification; carbamidomethylation of cysteins and monoisotopic peptide masses.

Real-time RT-PCR

For the quantification of Anx A4 mRNA in different ovarian cancer cell lines (CCC and SAC), we performed real-time RT-PCR. Total RNA was prepared from OVISE, OVTOKO, OVMANA, RMG-1 (CCC), OVSAHO and OVKATE (SAC) cell lines using an RNeasy Kit (Qiagen Valencia, CA) and cDNA was synthesized with a SuperScript™ III Reverse Transcriptase Kit (Invitrogen, Carlsbad, CA). A standard curve for Anx A4 cDNA was generated by the serial dilution of plasmid vector DNA, which encodes the Anx A4 gene. The primer sequences for Anx A4 were as follows: forward primer, 5′-ggaggtactgtcaaagctgc-3′ and reverse primer, 5′-gccactcagttctgacttcag-3′. Primers and cDNA were added to SYBR green premix (Invitrogen), which contained all the reagents required for PCR. The PCR conditions consisted of 1 cycle at 95°C for 1 min and 42 cycles of 95°C for 20 sec, 50°C for 20 sec and 72°C for 30 sec. PCR products were measured continuously with the My IQ™ Single-Color Real-Time Detection System (Bio-Rad Laboratories).

Western blotting

Cells and frozen tumor tissue samples were lysed in RIPA buffer (10 mM Tris-HCl, pH 7.5, 150 mM NaCl, 1% Nonidet P-40, 0.1% sodium deoxycholate, 0.1% SDS, 1 mM Na_3VO_4 and 1 × protease inhibitor cocktail (Nakalai Tesque)) followed by centrifugation (13,200 rpm, 4°C, 15 min), after which the supernatants were stored at −80°C until use. Protein concentrations were determined with the DC Protein Assay kit (Bio-Rad Laboratories), using BSA as the concentration standard. Extracted proteins were then resolved using 10% Bis-Tris Criterion XT Precast gels (Bio-Rad Laboratories) and subsequently transferred to PVDF membranes (Millipore, Bedford, MA). The membranes were washed and blocked with 1% skim milk in PBS containing 0.1% Tween 20 (PBST) and incubated with a goat polyclonal anti-Anx A4 antibody (sc-1930; Santa Cruz Biotechnology, Santa Cruz, CA) at a 1:300 dilution. Next, the membranes were incubated with horseradish peroxidase-conjugated donkey anti-goat IgG (Santa Cruz Biotechnology). Finally, the signals were visualized by means of an enhanced chemiluminescence (ECL) reaction system (Perkin-Elmer Life Sciences, Boston, MA). For loading control, western blotting and the subsequent antigen–antibody reaction were performed with GAPDH (Santa Cruz Biotechnology).

Immunohistochemistry

Expression of Anx A4 protein in ovarian cancer patient tissue sections was immunohistochemically measured with the ABC Kit (Vector Laboratories, Burlingame, CA). The total number of tissue section samples analyzed was 126 (43 CCC, 13 endometrioid, 8 mucinous, 62 SAC). Sections (3 μm) were prepared from formalin-fixed, paraffin-embedded tissue specimens, deparaffinized and rehydrated in graded alcohols. For antigen retrieval, the sections were incubated in a target retrieval solution (DAKO, Kyoto,